Ph.D. DISSERTATION

A study of photopatterning methods of silver nanowires and quantum dots for display application

디스플레이 응용을 위한 은나노 와이어 및 양자점의 포토 패터닝에 관한 연구

BY

LEE SEONWOO

AUGUST 2018

DEPARTMENT OF
ELECTRICAL AND COMPUTER ENGINEERING
COLLEGE OF ENGINEERING
SEOUL NATIONAL UNIVERSITY

A study of photopatterning methods of silver nanowires and quantum dots for display application

디스플레이 응용을 위한 은나노 와이어 및 양자 점의 포토 패터닝에 관한 연구

지도 교수 이 창 희

이 논문을 공학 박사 학위논문으로 제출함

2018 년 08월

서울대학교 대학원

전기정보 공학부

이 선 우

이선우의 공학 박사 학위논문을 인준함

2018 년 08월

위 원 장	이 신 두	(인)
부위원장	이 창 희	(인)
위 원	홍 용 택	(인)
위 원	이 진 균	(인)
위 원	배 완 기	(인)

Abstract

A study of photopatterning methods of silver nanowires and quantum dots for display applications

LEE SEONWOO
DEPARTMENT OF
ELECTRICAL AND COMPUTER ENGINEERING
COLLEGE OF ENGINEERING
SEOUL NATIONAL UNIVERSITY

For the most promising patterning method for silver nanowires and semiconductors which are in the quantum confinement regime, a well-established photolithography method can provide many advantages such as high productivity, high resolutions, and scalability for practical applications. However, there are many challenging problems applying these nanomaterials on photolithography process: materials stabilizing during patterning process, dispersibility in wet-coating solutions, physical delamination due to chemical & mechanical instability. In this study, newly designed formulations consisting of water-insoluble polymers (polymethylmethacrylate (PMMA)) that has excellent optical transparency with low refractive index and photosensitive cross-linking agents in organic solvents are proposed for silver nanowire patterning using sonication treatment. After UV curing under photomask and development with organic solvent, substrate was treated by simple water wash and short sonication to clean AgNWs in the unexposed areas. Finally, a fine pattern of AgNWs protected with a crosslinked polymer matrix was obtained. Based on this study, it turned out that the width of the obtained AgNW patterns was in the range of 100 μm to 3 μm, and it was confirmed that the protected AgNW network maintained excellent mechanical stability even after taping and bending tests. As applications, this method was applied to the organic transistor which is the core component of the future flexile electronic device. Compared to 0-D structures (e.g. spheres, clusters), one-

dimensional (1-D) nanowires with a high aspect ratio provide a better opportunity for connection between conductive materials when the electrodes are bent or elongated. To verify the usefulness of this patterning method, simple P3HT based organic field effect transistor was designed and fabricated, and then compared it with a reference device composed of Ag metal. For more applications to other nanomaterials, this study also proposes photopatterning methods of semiconductors which are in the quantum confinement regime. This study uses dispersion technology and binder chemistry. Studied dispersion methods with commercial dispersants and UV cross-linkable resins have verified high-loading QD blending and its photolithographic patterning applications. First of all, this study shows QD blending at low concentrations using QD powder and commercial dispersants. Then, it was further studied to prepare high loading QD blending (up to 30 wt.%) with additional additives. This QD formulations were tested to see its patternability and further confirmed changes in photophysical properties such as photoluminescence quantum yields (PLQYs), photoluminescence spectra, Full width at half maximum (FWHM), and optical properties retention during photolithography process. Finally, it shows a fine pattern images consisting of highly enriched QDs (20wt % and beyond), which can be potentially applied to color conversion films that converts blue light to red light or green light.

주요어: **photolithography, patterning, quantum dots, silver nanowire, UV curing**

학 번: 2015-31017

Contents

List of Figures

List of Tables

Chapter 1

Introduction

1.1. Overviews on Silver nanowires and Quantum dots

1.1.1. Silver nanowires (AgNWs)

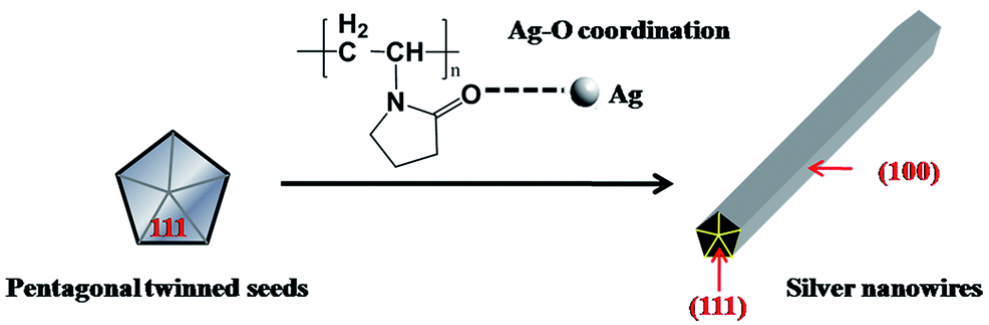

< Figure 1. Structure of AgNWs. [1] >

To date, metal nanowire in Figure 1 have attracted tremendous attention for the fabrication of transparent conducting electrodes (TCEs), and the resulting metal nanowire TCEs have been used successfully in organic solar cells and LEDs [2, 3]. Silver [4 - 7]. nanowire networks have been reported to behave as TCEs with comparable performance to ITO, along with bending and stretching stability. Based on the excellent electrical conductivity (6.3×10^7 S/cm) and high aspect ratio (length up to tenths of micrometers), silver nanowires (Ag NWs) are quite promising for transparent, highly conducting electrodes with mechanical flexibility [8]. In addition, several studies have indicated that a transparent electrode with a sheet resistance of *Rs* < 100 *ohm/sq* can be achieved easily. Lee et al. [9] pioneered the fabrication of Ag nanowire for TCE applications, they reported solution dispersed Ag nanowires from a polyol reduction method. In this case, the Ag nanowire

electrode revealed comparable electrical and optical performance to that of ITO, which can overcome the limitations of ITO mentioned above including the mechanical brittleness. In addition, their studies reported a simple drop casting method highlighting the possibilities for using highly scalable processing methodologies to reduce the processing costs significantly compared to those used for ITO. Random Ag nanowires networks allow the prospective generation of transparent conducting materials as a replacement for doped metal oxides. Owing to the association between the mechanical flexibility and small lateral diameters of Ag nanowires, transparent conducting films of Ag nanowires have superior electromechanically robustness to ITO films. These nanowire films are some of the premier candidates to supersede ITO films in optoelectronic applications, such as solar cells, displays, touch panels, organic light-emitting diodes (OLED), etc. Regarding the above aspects, the sheet resistance (Sheet resistance (*Rs*) and optical transmittance (*T* %) are two crucial parameters for assessing the performance of Ag nanowires, particularly for TCE applications. A low *Rs* with a high *T* value is always desirable.

In recent years, comprehensive characterization techniques have been carried out to examine the morphology and structure of Ag nanowires. Among these, scanning electron microscopy (SEM), transmission electron microscopy (TEM), and length and diameter tests have been used to track the morphological and structural variations of Ag nanowires. Kim et al. [10] reported Ag NWs prepared by a modified polyol synthesis, where KBr was added to the solution before adding $AgNO_3$, which results in competition for Ag^+ ions to reduce Ag^+ ions and form Ag nanowires. In addition, replacing the AgCl with NaCl seed can ensure that there will be no source of Ag present in solution before the addition of $AgNO_3$, which allows more accurate growth control of the nanowires. The high concentration of NaCl, compared to that of the Ag^+ ions from $AgNO_3$, contributes to the formation of nanoparticles instead of nanowires. On the other hand, it was possible to synthesize longer and thinner nanowires with a high yield when $AgNO_3$ are added in the process and resulted in high quality silver nanowires with a long aspect ratio.

The addition of nitrate anions (in the form of KNO^3) to the EG solution accelerated the formation rate and yield of Ag nanowires. In that study, short Ag

nanorods (Ag NR) with multiple twinned pentagonal crystalline structures can be assembled further with nanoparticles to form nanowires. The current nitrate-promoted self-assembly growth mechanism most likely becomes dominant at the later stages of a polyol reduction reaction and is responsible for the growth of long Ag nanowires. The presence of high concentrations of nitrate anions can promote the self-assembly of long AgNWs. Recently, uniformly interconnected AgNW networks [11] were synthesized using a modified polyol process, where Ag nanowires were produced by the reduction of $AgNO^3$ by EG in the presence of PVP and 1-butyl-3-methylimidazolium chloride (BMIM-Cl). The polyol method was modified by dispersing Ag nanowires in an exfoliated nanometer-sized clay platelets solution as the key element for increasing the viscosity of the solution and coating process of Ag nanowires. Hence, the nanowire networks were interconnected efficiently with improved spatial uniformity using BMIM-Cl. Modified synthetic methods allowed the formation of Ag nanowires with a relatively smaller diameter and longer length, thereby achieving a high aspect ratio (>1000). The as-synthesized Ag nanowires had diameters of 20 – 40 nm and lengths up to 20 – 40μm.

<Figure 2. Future technologies using AgNWs, from seminar on flexible electronics presented by Roshan Mani, 2015>

Among various applications of AgNWs, the utility of AgNW films, such as transparent electrodes in flexible displays in Figure 2, has been governed largely by

two critical parameters, sheet resistance and visible-light transmission. Either of these properties can be tuned individually to the desired value by changing the thickness of the Ag nanowire film. The sheet resistance and transmission decreased with increasing Ag nanowire film thickness. An effective transparent conductor should have high electrical conductivity and low absorption of visible light. Therefore, an appropriate quantitative measure of the performance of a transparent conductor can be expressed as follows:

$$T(\lambda) = \left(1 + \frac{188.5}{R_s}\frac{\sigma_{\mathrm{Op}}(\lambda)}{\sigma_{\mathrm{DC}}}\right)^{-2}$$

where *Rs* is the sheet resistance in ohms per square, *T* is the total visible transmission, $\alpha_{\mathrm{op}}(\lambda)$ is the optical conductivity and α_{DC} is the DC conductivity of the film [12]. Another figure of merit for transparent conducting materials was defined by Haacke,

$$\varphi_{\mathrm{TC}} = \frac{T^{10}}{R_s}$$

where *T* is the optical transmittance and *Rs* is the electrical sheet resistance. A large TC value indicates good performance of transparent conductors. In addition, *Rs* and *T* depends on the characteristics of the substrates.

The best quality of Ag nanowires on a glass substrate were obtained with a very low sheet resistance (*Rs* = 10.2 *ohm*/sq) and outstanding optical transmittance (89.9%).

1.1.2. Quantum dots

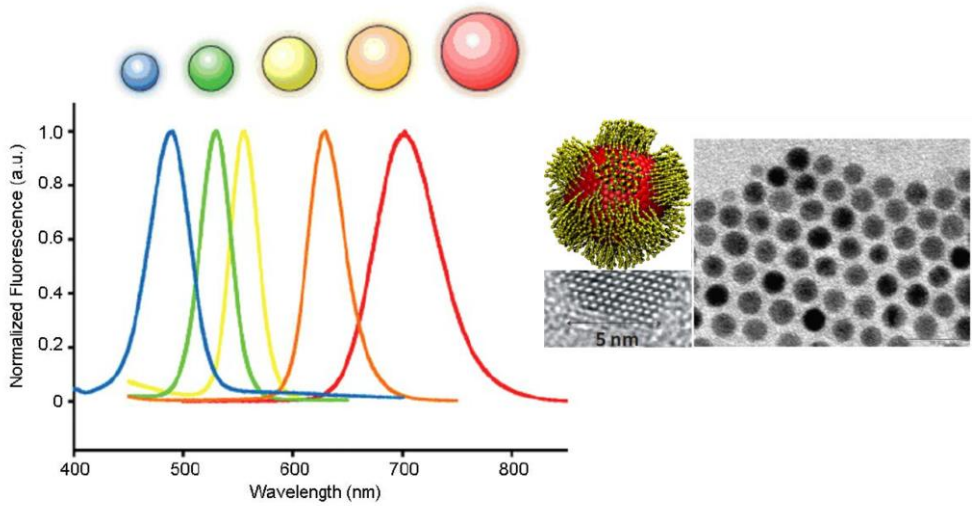

<Figure 3. TEM images of quantum dots presented by Prof. Bryan W. Boudouris, School of Chemical Engineering, Purdue University>

In Figure 3, quantum dots (QDs) [13 – 15] are semiconducting nanoparticles that exhibit unique optical and electronic properties. These materials can be synthesized in solution using relatively low temperature techniques [16 – 20]. Furthermore, because they can be suspended readily in solution, they can be collected and made into quantum dot inks or many types of compositions for a variety of applications using a highly efficient photoluminescence property.

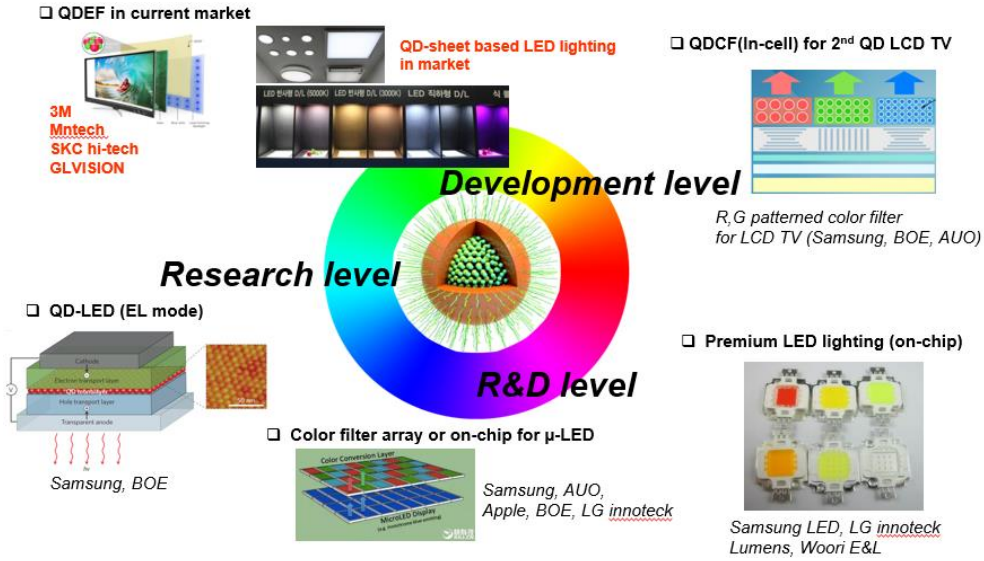

< Figure 4. Overview on ongoing works using photoluminescence >

To date, there have been intensive studies on quantum dots for display applications using photoluminescence property along with quantum dots based electroluminescent applications in Figure 4. As examples, color conversion films using quantum dots have been applied to liquid crystal displays (LCDs) and micro-LED technology.

Central to the technology on color conversion films is to use of the high-density colloidal QDs dispersion and is to do precise patterning without degrading the photophysical properties. In terms of colloidal QD dispersion, the key is to control the hydrophobic surface and the interaction with polar medium, since the required QDs composition is comprised of variety of binders such as poly-acrylates and other additives such as dispersants, stabilizers, and do on. In addition, these binders and additives are well soluble in polar vehicles such as PGMEA (propylene glycol monomethyl ether acetate). Particularly, uniformly re-dispersion of QDs in polar solvents is regarded as the most challenging problem since the organic molecules on the surface have strong hydrophobicity. To address these problems, various methods have been proposed such as ligand exchange [21 – 25], inter-chelated QDs with amphipathic polymers [26], thermodynamic ligand (referred as “entropy ligand”) [27], and chemical modifications via photoreactions [28] or catalysts [29].

However, surface modification methods can cause significant degradation of QDs in terms of color purity and photoluminescence quantum efficiency during surface modifications, limiting its potential applications. Due to these reasons, preferably, as synthesized QDs need to be directly used without any surface modifications. And we have also found that as-prepared QD is commonly dissolved in non-polar medias such as hexane, chloroform, and toluene that needs additional solvent exchange steps. This solvent exchange has also another problem in terms of scalability, limiting its potential applications in terms of scalability in industry. Among the recent QDs applications [30 – 32], Qibing Pei et al [33] has proposed an in-situ copolymerization method for ultra-high-loading QDs-composites (up to 60 wt.%) using ligand exchange method, but nothing has been discussed the solvent issue.

1.2. Challenging Problems in Patterning

1.2.1. Silver nanowires (AgNWs)

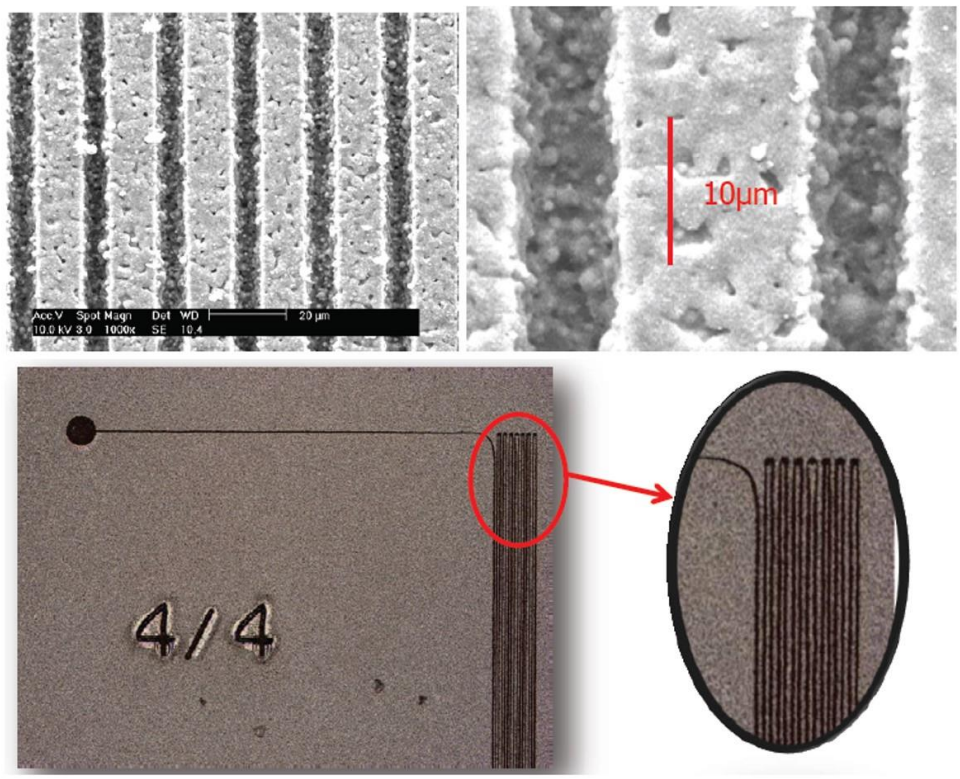

< Figure 5. SEM images of patterns: smallest line width/spacing demonstration, by Bob Hainsey et al, 2013 >

In recent years, in addition to the conventional photolithography method [34 – 36], there have been proposed many patterning methods such as dry transfer technology [37], intense pulsed light irradiation [38], laser direct write patterning [39, 40], gravure [41, 42], and inkjet method as a printing technology [43]. Among them, laser direct writing patterning in Figure 5 is being used in the industry with several advantages such as high resolution and fast process. However, this technique has the disadvantage of high manufacturing cost due to expensive laser equipment and moderate productivity.

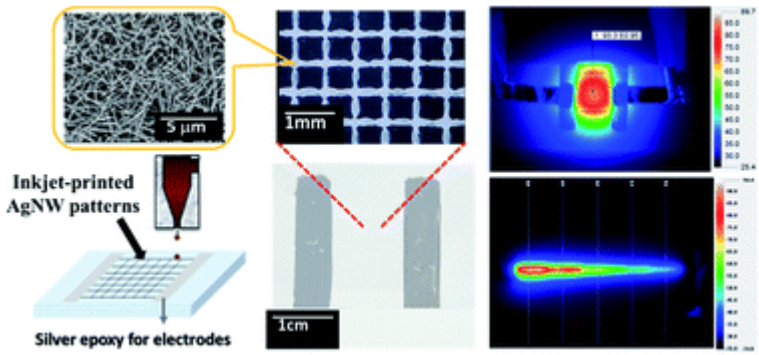

< Figure 6. Direct printed silver nanowire thin film patterns, by Ying-Chih Liao et al., RSC Advances, 2015 >

In addition, the printing technology is easy and the manufacturing process is simple, but there are problems such as low productivity, low resolution, and clogging in inkjet printing in Figure 6.

In contrast, photolithography is the most preferred technology due to its high productivity, high resolution, and high scalability. However, it has been found that, when AgNWs are patterned by photolithography, photoresist and wet chemical etchants are not suitable for AgNWs patterning due to physical exfoliation during PR strip and changes in sheet resistance due to corrosion. To address these problems, photocuring methods using commercial negative photoresists (e.g. SU-8) [44], UV curable aqueous resins, AgNW / polymer compositions [45] have recently been developed. The photocuring method not only simplifies the patterning process, but also protects the AgNW network simultaneously without the use of photoresist (PR) and strippers. However, a chemical etchant is still required to clearly remove the AgNWs with respect to the high resolution patterns (width: < 20 μm, line space: < 20 μm). Recently, Kim et al. [46] proposed a photosensitive AgNWs complex that creates an electrical path without using an etchant. On the other hand, it still needs improvement to avoid electricity shortages. As a result, there is still strong demands for patterning methods without the use of a wet chemical etchant during photolithography.

1.2.2. Quantum dots (QDs)

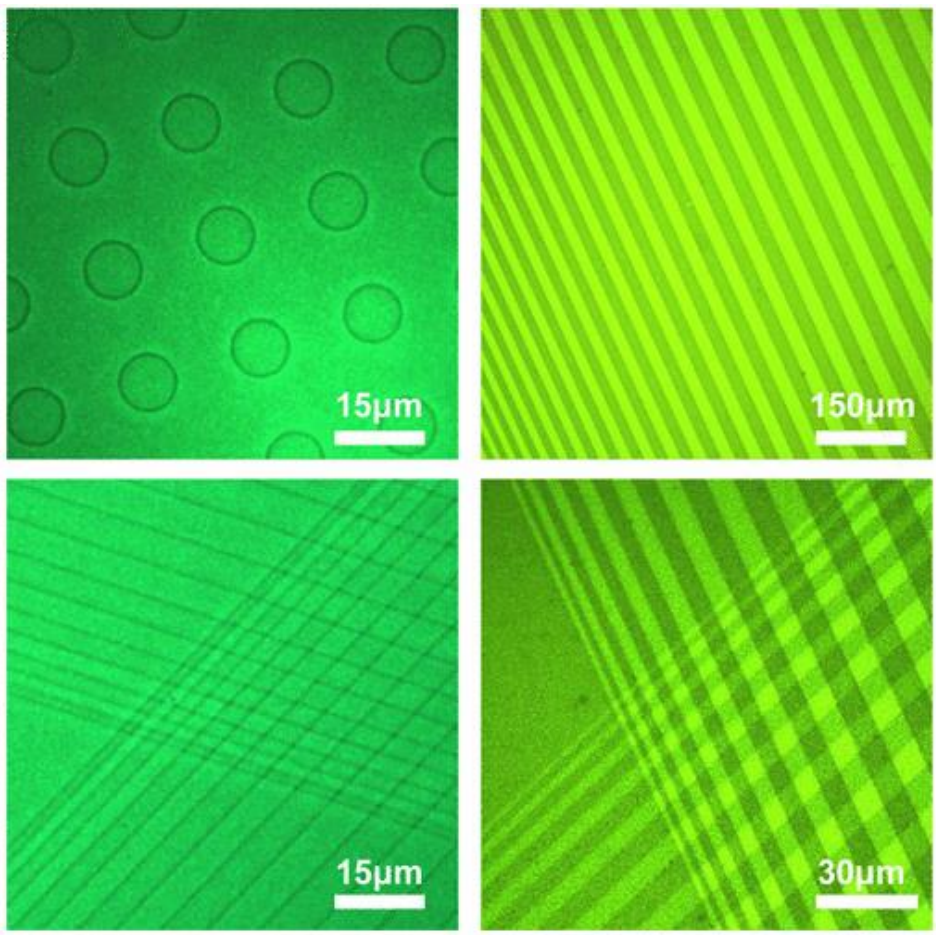

< Figure 7. QD patterns by interference lithography assisted microstamping method proposed by Prof. Vladimir V. T >

Recently, some QD patterning methods such as ink-jet printing, stamping, and photolithography have been reported. Among them, ink-jet printing has been shown very promising results in terms of manufacturing cost with minimized fabrication processes. However, some roadblocks such as low productivity, reliability in process, limited resolutions have been regarded as challenging problems for practical applications. As alternative solutions, photolithography process and related technologies have been intensively studied. For example, Vladimir V. Tsukruk et al [47] in Figure 7 has recently proposed high-resolution quantum dot photopatterning via interference lithography assisted microstamping.

This patterning method has shown that a QD composition after surface modifications can be readily patterned. Author has shown that the patterned QD images down to microscale can be easily prepared. However, stamping method still needs to improve some points to be applied to practical applications. For example, reliable stamping equipment and processing have to be further improved for high productivity and manufacturing cost.

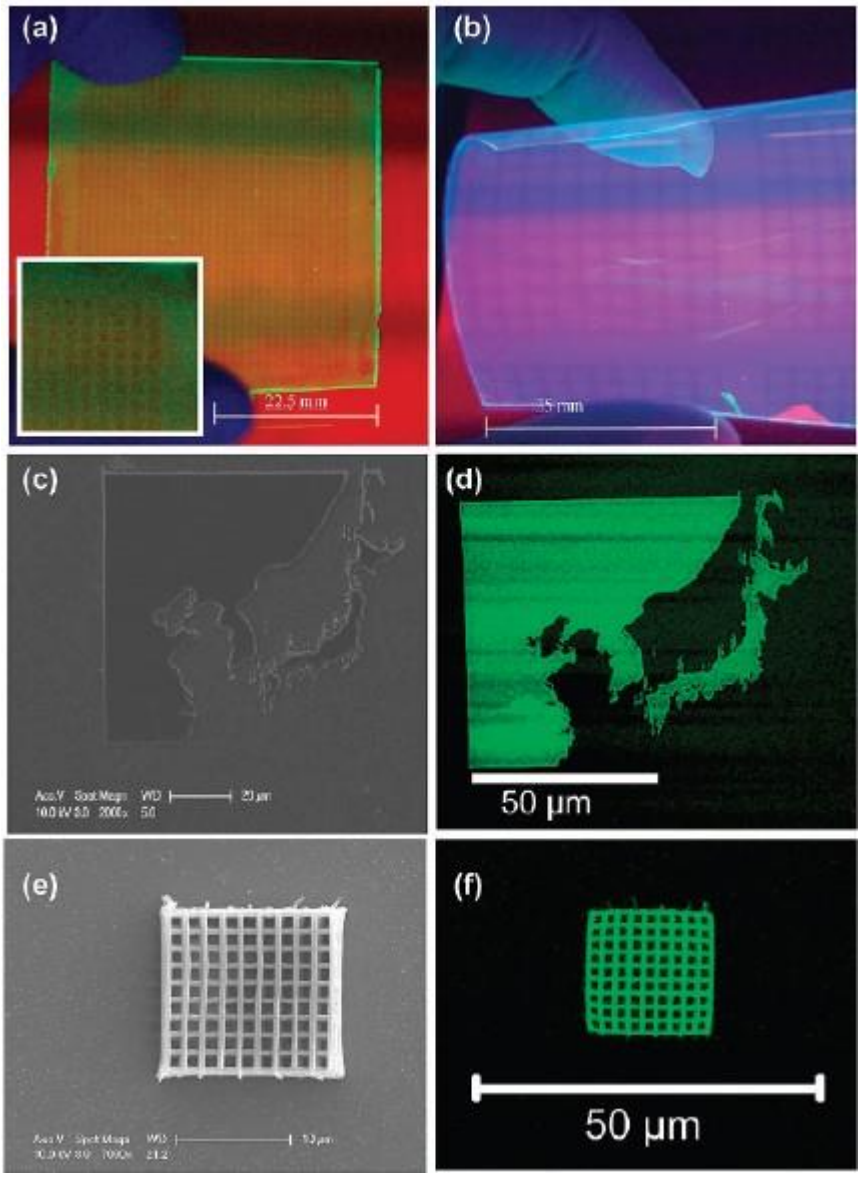

< Figure 8. QD patterns by photolithography methods using surface modified QDs. proposed by Samsung Advanced Institute of Technology, 2010, ACS>

Kwang-Sup Lee et al [48] has also recently demonstrated photolithographic QDs patterning using photofunctionalized QDs. It has been revealed that well-established photolithography using surface modified QDs can be able to produce QD images down to microscale. However, surface modified QDs can be readily degraded in terms of photoluminescence properties such as PLQYs, PL shift during

the surface modifications.

On the basis of our analysis, photolithography process is the most promising method in terms of productivity, resolution, reliability in process. However, it still needs improvement. it is concluded that industry still demands for more simplified blending methods for high loading of QD compositions, which is capable of photolithographic patterning.

1.3. Outline of Thesis

Firstly, this study proposes an etchant-free photolithographic patterning method using transparent UV curable PMMA resin and ultra-sonication for AgNWs patterning.

Secondly, this study proposes a method of high-density of quantum dots (QDs) dispersion for potentially color conversion films.

Finally, finely patterned each material are applied for display applications.

This thesis is divided into five chapters.

In ***Chapter 1***, general overviews on silver nanowires and quantum dots were mentioned. Then, challenging problems patterning were also overviewed.

In ***Chapter 2*** discuss key concepts: photolithography, sonication, direct cross-linking polymers, and quantum dots dispersion. In addition, materials, formulations, and device fabrications are also discussed.

In ***Chapter 3***, fine AgNWs patterning via sonication and evaluated electrical, mechanical, and optical properties are discussed. In addition, application of patterned AgNWs on organic transistor as source / drain electrode is discussed.

In ***Chapter 4***, QDs dispersion, evaluations of photophysical properties are discussed. And photolithographic fine QD patterning with high density are described.

In ***Chapter 5***, conclusion is given.

Chapter 2. Key Concepts and Experiments

2.1. Photolithography

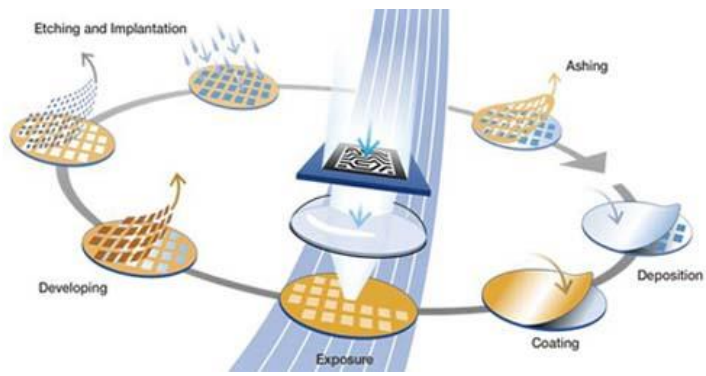

< Figure 9. Overall conventional photolithography: www.ASML.com>

Photolithography in Figure 9 is a technology for transferring the shadow of a desired pattern onto a wafer called a mask, which is made of a metal pattern on a glass plate, and transferring the shadow onto a wafer. For example, a semiconductor device is a three-dimensional structure, but a circuit such as CAD can be designed by dividing a complex structure into two-dimensional layers according to respective heights. If you draw these two-dimensional circuits with a pen, it will take a lot of time. However, it is possible to mass-produce the devices in a short time by repeating the same patterns repeatedly using light after manufacturing one disk of photomask accurately. Of course, not only the photolithography process does not produce a three-dimensional structure, but it can be combined with other unit processes such as thin film deposition and etching, and a selective protective film can be formed through the lithography process to enable partial etching.

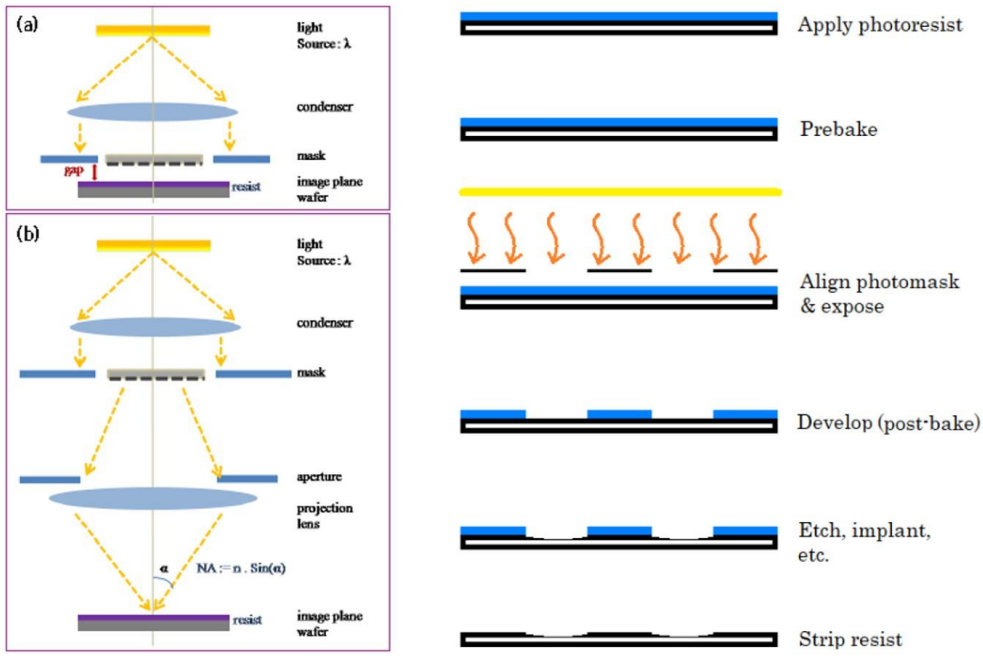

< Figure 10. Schematic diagram of photolithography systems. (a) proximity printing. (b) Projection printing >

The basic form of photolithography equipment that uses light to light is determined according to the optical system used, and there are roughly divided exposure and projection exposure methods in Figure 10.

In the early days of semiconductor production, contact printing or proximity printing method was used. These two methods are classified according to the gap between the mask and the wafer. In general, the mask and the wafer are uniformly in close contact with each other, It is at the core of technology that positive light reacts evenly with photoresist. However, in the case of the contact type, there is a disadvantage in that the life of the mask is shortened due to the presence of the photosensitizer. In addition, the proximity exposure also causes a drastic decrease in resolution and reproducibility due to the gas generated in the photosensitizer during exposure. Therefore, projection printing has been used as a main technology of semiconductor and LCD manufacturing, which has advantages of long mask life, high resolution, and high productivity.

2.2. Sonications

Ultrasonic cleaning in Figure 9 is a process that uses ultrasound (usually from 20–400 kHz) and an appropriate cleaning solvent (sometimes ordinary tap water) to clean items. The ultrasound can be used with just water, but use of a solvent appropriate for the item to be cleaned and the type of soiling present enhances the effect. Cleaning normally lasts between three and six minutes, but can also exceed 20 minutes, depending on the object to be cleaned [49].

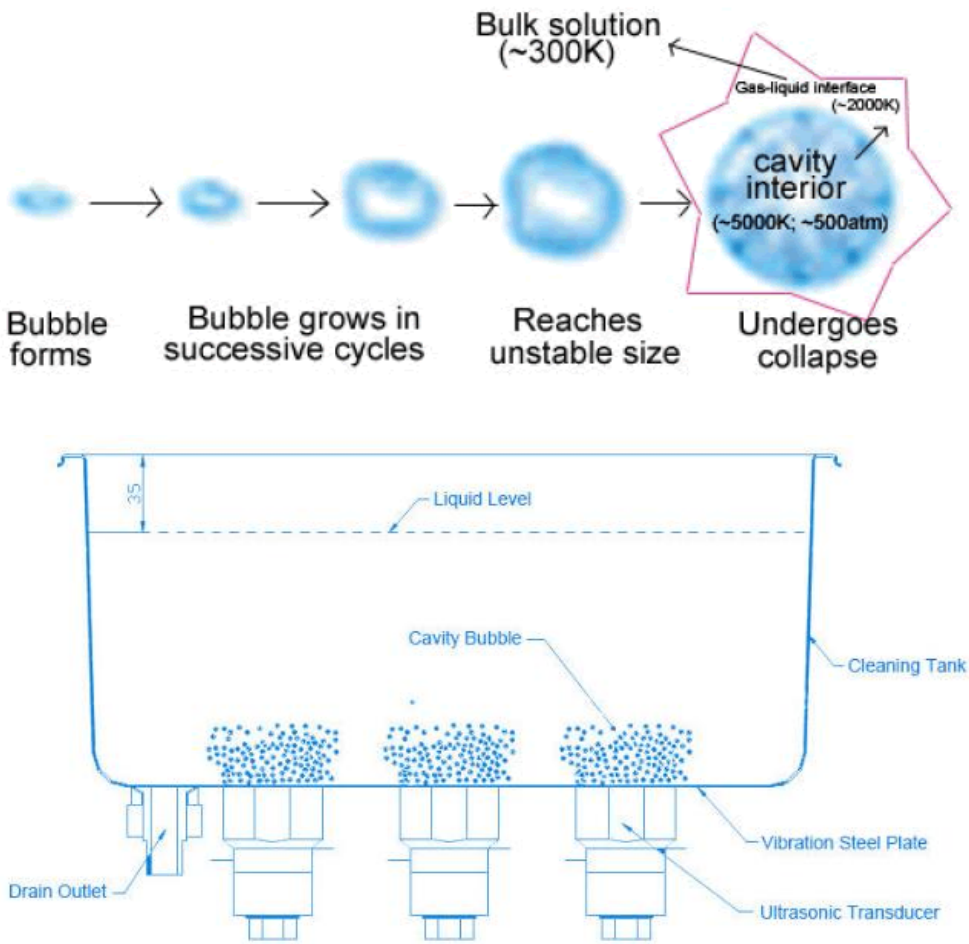

< Figure 11. Basic principle of operation of sonication process >

Ultrasonic cleaning uses cavitation bubbles induced by high frequency pressure (sound) waves to agitate a liquid. The agitation produces high forces on contaminants adhering to substrates like metals, plastics, glass, rubber, and ceramics. This action also penetrates blind holes, cracks, and recesses. The

intention is to thoroughly remove all traces of contamination tightly adhering or embedded onto solid surfaces. Water or solvents can be used, depending on the type of contamination and the workpiece. Contaminants can include dust, dirt, oil, pigments, rust, grease, algae, fungus, bacteria, lime scale, polishing compounds, flux agents, fingerprints, soot wax and mold release agents, biological soil like blood, and so on. Ultrasonic cleaning can be used for a wide range of workpiece shapes, sizes and materials, and may not require the part to be disassembled prior to cleaning [50]. Objects must not be allowed to rest on the bottom of the device during the cleaning process, because that will prevent cavitation from taking place on the part of the object not in contact with solvent [51].

In an ultrasonic cleaner, the object to be cleaned is placed in a chamber containing a suitable solution (in an aqueous or organic solvent, depending on the application). In aqueous cleaners, surfactants (e.g., laundry detergent) are often added to permit dissolution of nonpolar compounds such as oils and greases. An ultrasound generating transducer built into the chamber, or lowered into the fluid, produces ultrasonic waves in the fluid by changing size in concert with an electrical signal oscillating at ultrasonic frequency. This creates compression waves in the liquid of the tank which 'tear' the liquid apart, leaving behind many millions of microscopic 'voids' or 'partial vacuum bubbles' (cavitation). These bubbles collapse with enormous energy; temperatures and pressures on the order of 5,000 K and 135 MPa are achieved; [52, 53] however, they are so small that they do no more than clean and remove surface dirt and contaminants. The higher the frequency, the smaller the nodes between the cavitation points, which allows for cleaning of more intricate detail. Ultrasonic transducers showing ~20 kHz and ~40 kHz stacks. The active elements (near the top) are two rings of lead zirconate titanate, which are bolted to an aluminium coupling horn. Transducers are usually piezoelectric (e.g. made with lead zirconate titanate (PZT), barium titanate, etc.), but are sometimes magnetostrictive. The often harsh chemicals used as cleaners in many industries are not needed, or used in much lower concentrations, with ultrasonic agitation. Ultrasonics are used for industrial cleaning, and also used in many medical and dental techniques and industrial processes

2.3. Principle of UV curing and systems

Photoinitiator based curing method

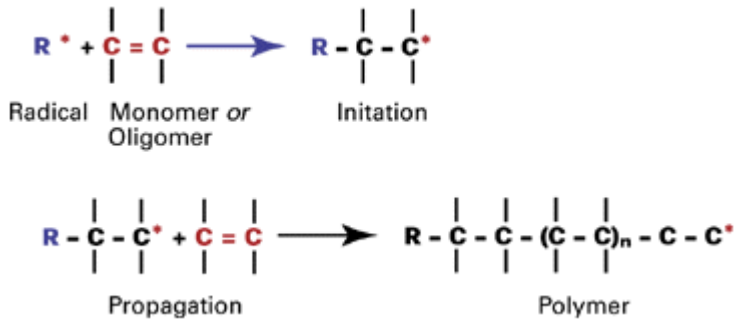

< Figure 12. Example: Basic Free-Radical Polymerization >

To start the reaction, it is necessary to use UV initiators, sometimes in combination with UV sensitizers. The UV initiators form free-radicals. As is the case for other free-radical polymerization reactions, atmospheric oxygen inhibits polymerization, primarily on the upper film layers. In practice, curing is effected by a compromise of mainly UV light of longer wavelengths (315 to 380 nm), complemented with additional, smaller amounts of UV light of wavelengths below 315 nm. This smaller portion guarantees that the surface of the film will be cured efficiently and decreases the inhibitory effect of oxygen.

As the energy density of UV light is inadequate for the polymerization reaction, photoinitiators and sometimes photo-sensitisers have to be used. The UV light transforms the reactive group of an UV absorber or a UV sensitiser into an excited state. The excited molecules form free-radicals by cleavage of bonds or by adding hydrogen atoms.

The free-radicals trigger free-radical polymerization at the double bonds of the ingredients of the UV system. The reactions are the same as those which take place when peroxy initiators are used. Here, too, the sequence is initiation, chain propagation, chain termination by re-combination, free-radical transfer or disproportionation. However, in the case of UV curing, there is a possibility of side-reactions by deactivation of initiator molecules and emission of light (fluorescence or phosphorescence) or by reaction with free-radical scavengers. Direct recombination of initiator free-radicals may also take place and the aforementioned inhibition by oxygen of air.

In general resin systems which is cured by UV-light may consist of the following ingredients, where the first three are found in almost all formulations.

(i) Prepolymer (or oligomers)
(ii) Diluents (or monomers)
(iii) Photoinitiator
(iv) Coinitiator
(v) Light stabiliser
(vi) Thermal stabiliser
(vii) Colourants, plasticisers and additives

It can be further classified as follows
(i) Unsaturated polyester/acrylated polyester
(ii) Acrylated epoxy resin
(iii) Acrylated urethanes (both aliphatic and aromatic)
(iv) Acrylated silicone resins
(v) Acrylated polyethers
(vi) Acrylated melamines
(vii) Acrylated oils
(viii) N-vinyl urethanes
(ix) Thiolene system

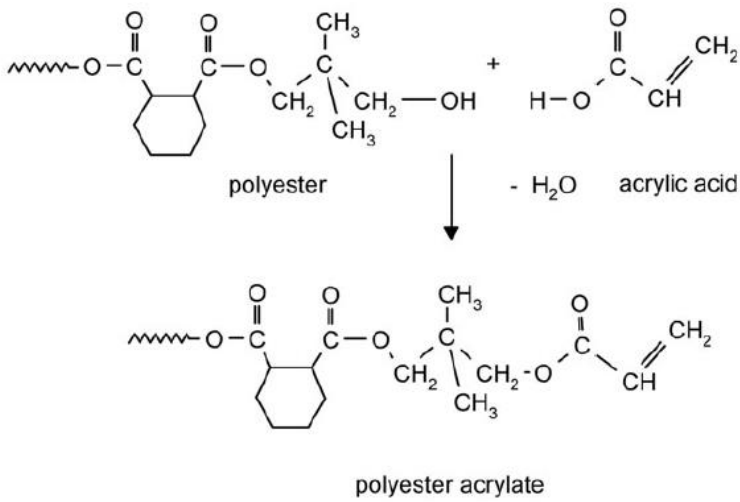

< Figure 13. A structure of polyester acrylates >

From the classifications, this study has employed unsaturated polyester/acylated polyester because some of advantages. Polyester acrylates in Figure 13 can be produced in a wide range of viscosities and reactivities to adopt to end uses in printing inks, wood and paper coatings. One of the major advantages offered by polyester acrylates over the other prepolymers is their low viscosity for example the basic recipe reported by Rybny has a viscosity of 1:660 centipoise at a molecular weight of around 1000 compared with an epoxy acrylate which will be 5-10 time higher in viscosity.

No.	Cured films	Acrylic	Polyester	Urethane	Epoxy
1	Tensile strength	Low	Moderate	Variable	High
2	Flexibility	Good	Variable	Good	Poor
3	Chemical resistance	Low	Good	Good	Excellent
4	Hardness	Low	Moderate	Variable	High
5	Non yellowing	Excellent	Poor	Variable	Moderate to Poor

< Table 1. General film properties of UV cured acrylated oligomers >

2.4. Dispersion of QD powder by dispersants

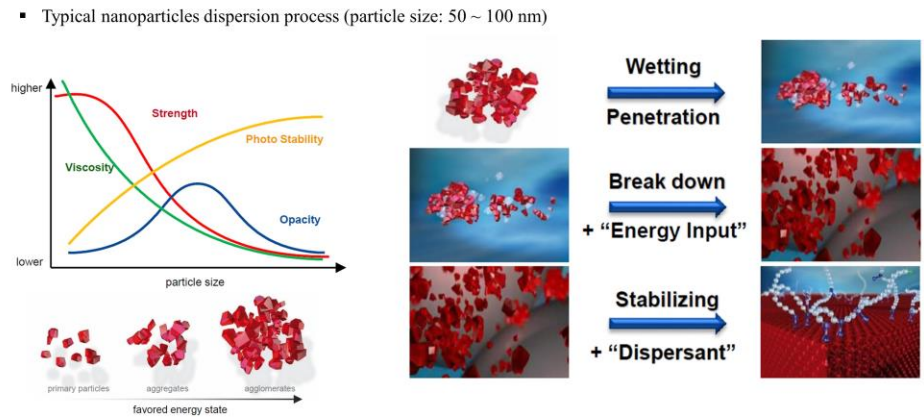

< Figure 14. Typical process of dispersing nanoparticles (e.g. pigment), BASF >

A colloidal suspension is characterized by its behavior that the finely divided small particles do not settle under the force of gravity.

The Dispersion process can be divided into three individual steps in Figure 14:

1. Wetting of the pigment particles by the fluid components of the mill base
2. Breakdown of the associated particles (agglomerates and aggregates) leading to smaller particle sizes
3. Stabilization of the dispersion preventing renewed association (flocculation)

Pigment particles can be divided into three classes:

i. Primary particles = crystal
ii. Aggregates = Primary particles with surface to surface conatct
iii. Agglomerates = Primary particles touching each other via edges and corners

Pigments are classified according to their chemical nature as organic and inorganic pigments. Inorganic pigments are usually coarser than organic pigments, with the exception of carbon blacks and a few special pigment types, such as transparent red oxides. The diameter of the primary particles of inorganic pigments usually ranges between 0.2 and 0.5 microns; while organic pigments lie between 0.03 and 0.08 microns.

2.5. Materials

2.5.1. Photosensitive QD Formulations

Cadmium oxide (99.99% trace metal basis, Aldrich), zinc acetate dehydrate (99.99% trace metal basis, Aldrich), oleic acid (technical grade, 70%, Aldrich), oligomer (PO 94F, BASF), dipropylene glycol diacrylate (BASF), Irgacure® Oxe01 (BASF), 1-octadecene (technical grade, 90%, Aldrich), sulfur (99.998% trace metal basis, Aldrich), trioctylphosphine (97%, Aldrich), tetrahydromethylammonium hydroxide pentahydrate (TMAH $5H_2O$, > 97%, Aldrich), Selenium powder (100 mesh, 99.99% trace metals basis, Aldrich), propylene glycol monomethyl ether acetate (PGMEA, > 99.5%, Aldrich) were purchased and used as received. All common solvents used were ACS grade. CdSe@ZnS core−shell QDs were synthesized following a well-developed protocol [54].

In a typical experiment, purified and washed QDs was dried in a vacuum for 3 hours and stored in air before using. 300 mg of dried QDs were mixed with 100 mg of dispersants and 200 mg of an oligomeric binder were added by 100 mg of PGMEA. The mixtures were mixed by a shaker for 5 hours at 70°C. After dissolving QDs clearly, a prepared cocktail comprised of 300 mg of mixture (30 % : 15 % : 1.0 % : 44 % = PO94F : DPGDA : Irgacure® Oxe01 : PGMEA) were added to the mixture and blended for further several hours at room temperature in the dark. The prepared photosensitive QD compositions were filtered through a 450 nm pore-size PTFE syringe filter to remove the remained minimal precipitates.

First, acetone, water, and IPA were used for cleaning glass substrate. The photosensitive QD compositions were spin coated (2000 rpm, 10 seconds) on the cleaned glass substrate. The QD layer was baked for 1 min at 100°C and exposed to

i-line for 2 seconds (i-line, Karl Suss MJB3 UV400 mask aligner) under a photo-mask. After UV irradiation, subsequently, the layer was developed by sole PGMEA for 30 seconds and rinsed by water. Finally, the patterns were further baked at 180 ^{o}C for 30min.

The QD film thickness was measured by DektakXT (BRUKER). UV−visible tests were performed on a Shimadzu UV-1800 spectrophotometer. Optical images were obtained by AxioCam HRc, ZEISS. The PL spectra and photoluminescence quantum yields (PLQYs) were measured by Quantaurus-QY Absolute PL quantum yield spectrometer (C11347-12, Hamamatsu). Typically, photoluminescence quantum yields of the QDs in chloroform were measured by the relative method [55], with Rhodamine-6G (R-6G) in Ethanol (PLQY = 0.95, O.D = 0.05) serving as the reference standard. In short, photoluminescence (under 450 nm excitation) and absorbance spectra were recorded for a series of dilute solutions having different optical density (0, 0.15, 0.30, 0.50, 0.70, 0.90, respectively). The integrated PL intensities were plotted against the absorbance at 450 nm for both QDs and R-6G solutions.

2.5.2. Photosensitive Resins for AgNWs patterning

1.0 wt % of AgNWs dispersion in IPA with an average diameter (25 nm ± 5 nm) and length (100 μm ± 5 μm) were purchased from Nanopyxis cop., and it was further diluted. P3HT (Sepiolid^{TM}, P200, M_W: < 5,000, supplied by BASF SE), PET film (thickness: 125 μm, supplied by SKC Films), PES film (thickness: 30 m, supplied by BASF SE), PMMA (poly(methyl methacrylate, M_W: 150,000 from Sigma Aldrich), Triton X-100 (M_W: 647, from Sigma Aldrich), HPMC (Hydroxypropyl methylcellulose, Mn ~ 90,000 from Sigma Aldrich), Photosensitive cross-linkers (supplied by BASF SE), Poly(1-vinylpyrrolidone-co-vinyl acetate, average M_W: ~ 50,000, from Sigma Aldrich), Ag metal (99.99% trace metals basis, from Sigma Aldrich). All solvents were purchased from Sigma Aldrich and used without purification.

Transparent PET film (thickness: 125 μm) was used as the substrate. Before fabrication, the PET film was washed with water, acetone, and IPA with ultra-sonication treatment for 15 minutes, respectively. 0.2 wt.% AgNWs ink (see stock formulation) was deposited on the substrate by doctor blading coater (coating speed: 20 mm/s, and 25 μm in highest, ZAA 2300, from ZEHNTNER testing instruments), and then the layer was dried in vacuum oven (at 100^{o}C) for one minute. After cooling down to room temperature, UV curable PMMA resin was coated on the dried AgNWs. After placing a photo-mask, the films were exposed with a Karl Suss MJB3 UV400 mask aligner for an exposure dose of 49 mJ/cm^2 (i-line, 365 nm) for 2 seconds. Finally, the UV cured films were developed for one minute in butyl acetate, and then it was rinsed by water, baked for 60 seconds at 100^{o}C, and finally treated by ultra-sonication in water within 30 seconds.

Transparent UV curable PMMA resin (1.0 wt.%): 10mg of PMMA polymers and 300 mol% of photosensitive cross-linker based on used PMMA contents were together dissolved in a 1:1 mixture of ethyl acetate and butyl acetate (0.99 g). Other

concentrations were prepared in the same manner as described above. The resin was stored at room temperature before using.

0.2 wt.% AgNWs ink: 2g of AgNWs dispersion (1.0 wt.% in IPA) was mixed by 200 mg of HPMC as binders and 25 mg of Triton X-100 as surfactants. The mixture was further diluted by 7.875 g of IPA.

2.6. Device Fabrications

The patterned AgNWs on PET film was treated by water, acetone, and plasma treatment with the argon gas as cleaning process. The P3HT dissolved in 1,2-dichlorobenzene (10 mg/mL) was deposited by spin-coating method (2,000 rpm, 30 seconds) and baked in vacuum oven at 90 ^{o}C for 12 hours. The thickness was around 50 nm (measured by DektakXT, BRUKER). Then, polyvinylpyrrolidone-vinyl acetate polymer dissolved in butyl acetate (70 mg/mL) was deposited by spin coating method (2,000 rpm, 60 seconds, around 600 nm). Finally, silver metal as a gate electrode (0.1 nm/s, 50 nm) was deposited by thermal evaporation. The transfer and output curves were measured by MST-1000H, from MS TECH).

2.7. Evaluations

Optical transmittance was recorded by UV-visible spectrometer (UV-1800, Shimadzu) in the 300-800 nm wavelength range. The sheet resistance was measured by a noncontact measurement system (Napson Corporation, EC-80P, Japan). Bending test (JIBT-610, radius bending tester) was implemented at 2.0 mm bending radius. The changes in sheet resistance were recorded during inward and outward bending cycles. The surface roughness was measured by AFM using an OLTESPA-R3 cantilever from Bruker with a tapping mode. Optical images are obtained from AxioCam HRc, ZE

Chapter 3. AgNWs Patterning by Sonication

3.1. AgNWs patterning process & optical property

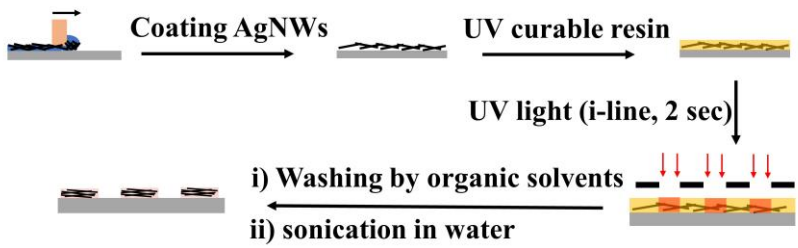

< Figure 15. A schematic illustration coating and patterning process using a UV curable resin >

According to Figure 15 and 16, a patterned transparent conductive film having a transmittance of about 81% and a sheet resistance of 19.1Ω / sq was made into a doctor blade coater with 0.2 wt.% AgNWs ink and dried for a minute. We then considered UV curable PMMA resins that require a photosensitive cross-linker. Fortunately, photosensitive cross-linkers have been provided and blended by commercial PMMA polymers in organic solvents. The cross-linking mechanism is assumed to be "alkyl CH insertion by nitrene mediated photocross-linking reactions" as described in literature [56]. In the case of PMMA polymers, we believe that the alkyl groups of PMMA polymers can be directly crosslinked by

known alkyl CH insertion. The prepared UV-curable PMMA resin was coated on silver nanowires on a PET film. After irradiation by UV light (i-line) with a photomask, unexposed areas were developed with butyl acetate for a minute. Finally, we conducted ultra-sonication in water for 30 seconds to remove clearly AgNWs in unexposed areas.

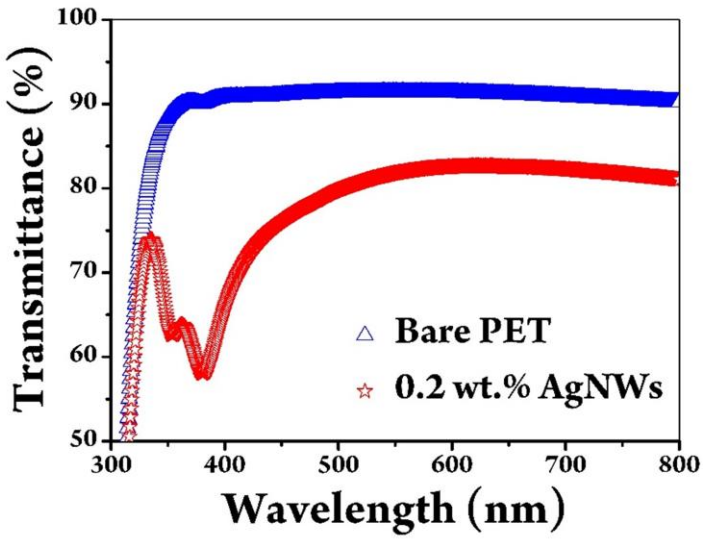

< Figure 16. A representative optical transmittance of AgNWs coated PET films >

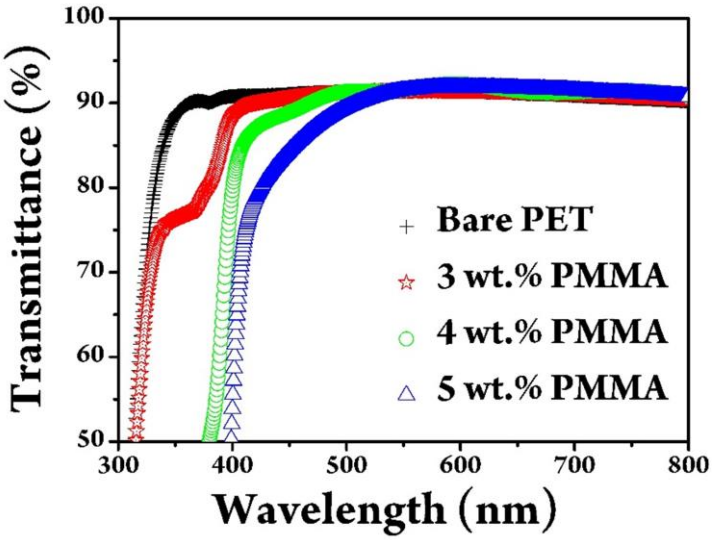

< Figure 17. Transmittance of UV cured resins with different PMMA content: 3 wt. % PMMA, 4 wt.% PMMA, and 5 wt.% PMMA >

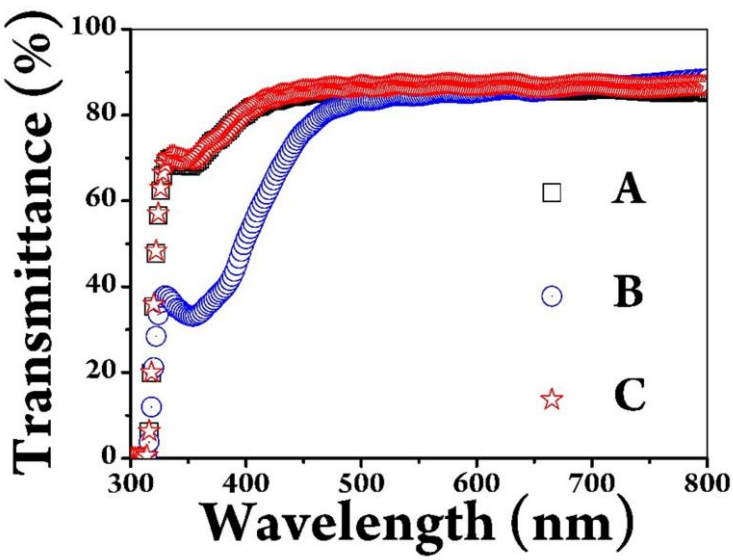

< Figure 18. Recovery of transmittance of UV cured resins by washing butyl acetate, A: as coated AgNWs, B: as coated AgNWs and UV curing, C: washed by butyl acetate after UV curing >

In order to confirm the change of the transmittance by the UV-curable resin, we first examined three different formulations of PMMA in Figure 17. After UV irradiation for two seconds, the transmittance of the film coated with PMMA formulations (4.0 wt.%, 5.0 wt.%) showed a significant decrease at a wavelength in the range of 350-500 nm. We estimated that a decrease would occur due to the increase in the concentration of by-products resulting from the cross-linking agents and the unknown radical reactions of the PMMA polymers during UV irradiation. We then found that the optical transmittance of TCF coated by 3 wt. % PMMA can be fully restored by developing with butyl acetate in Figure 18.

3.2. Comparison of water rinsing and sonication

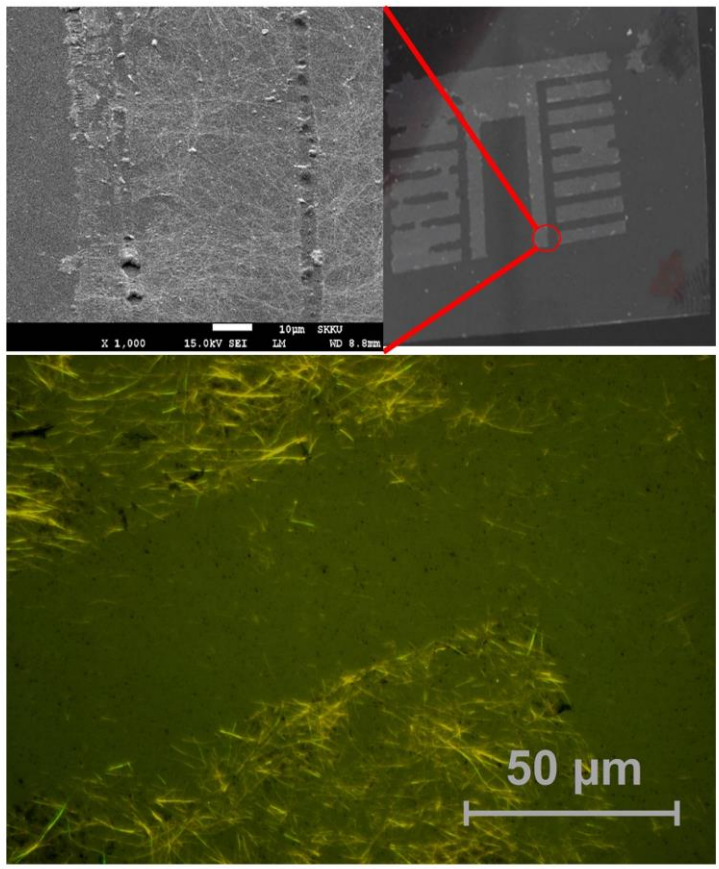

< Figure 19. Optical microscopy images of AgNWs removal tests after developing with organic solvents, simple water rinsing >

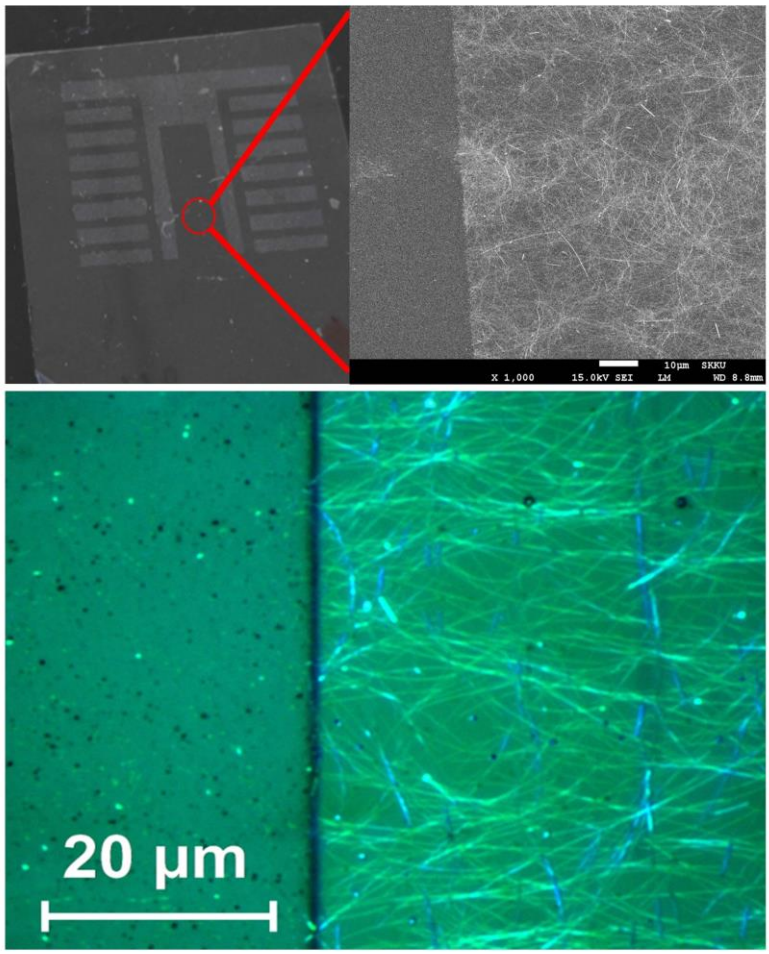

< Figure 20. Optical microscopy images of AgNWs removal tests after developing with organic solvents, ultra-sonication in water >

After developing, we attempted to remove the AgNWs from the unexposed region through simple water flushing. However, we have realized that water flushing is not suitable to remove AgNWs clearly in Figure 19. Next, we have considered to use short ultra-sonication in water. we have found that ultrasonic processing can remove AgNWs clearly and more effective for fine patterns up to 5 μm even though fine patterns could be a little damaged. A more detailed optical microscope images with scanning electron microscopy (SEM) is shown in Figure 20. To confirm the usefulness of our ultra-sonication method, we investigated more diverse fine AgNW patterns. As a result, it came to conclusion that it is very useful

for fine patterns up to 20 μm and we have explored a variety of AgNWs patterns in Figure 21.

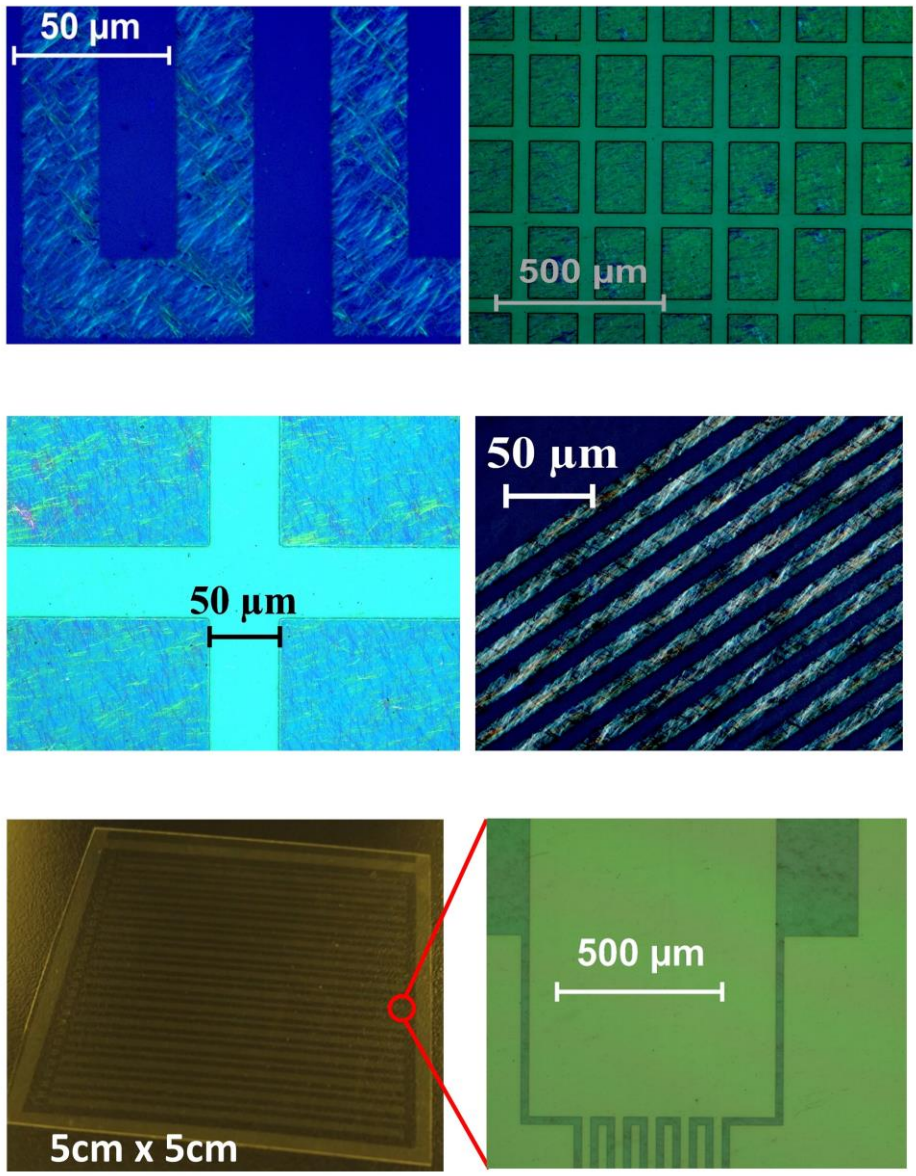

< Figure 21. Optical microscopy images of patterned AgNWs images by using ultra-sonication in water >

3.3. Mechanical Stability

3.3.1. Taping Test / Bending test

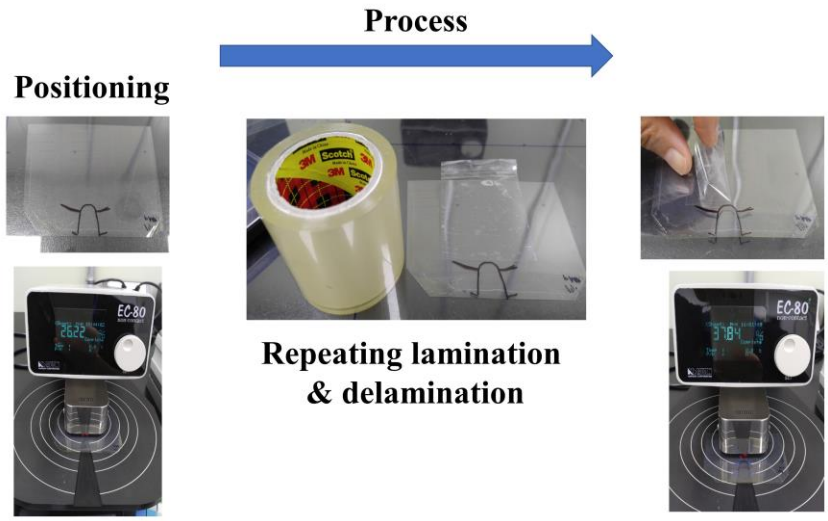

< Figure 22. A schematic illustration repeated taping tests with 3M Scotch tape >

Another new issue is the detachment of AgNWs due to its poor adhesion property on films. To confirm the adhesion to specific substrates (PET, PES), UV curable resins with different PMMA contents were prepared and peel test was performed with 3M Scotch tape to confirm the adhesion property in Figure 22.

In Figure 23 and 24, we examined two representative polymers: one is commercial polystyrene (PS, MW: 100,000), another is polymethyl methacrylate (PMMA, MW: 150,000). As can be seen, we confirmed that PMMA based protection on AgNW network shows better adhesion power to PS based matrix. We think that PMMA is stronger interaction with PET film.

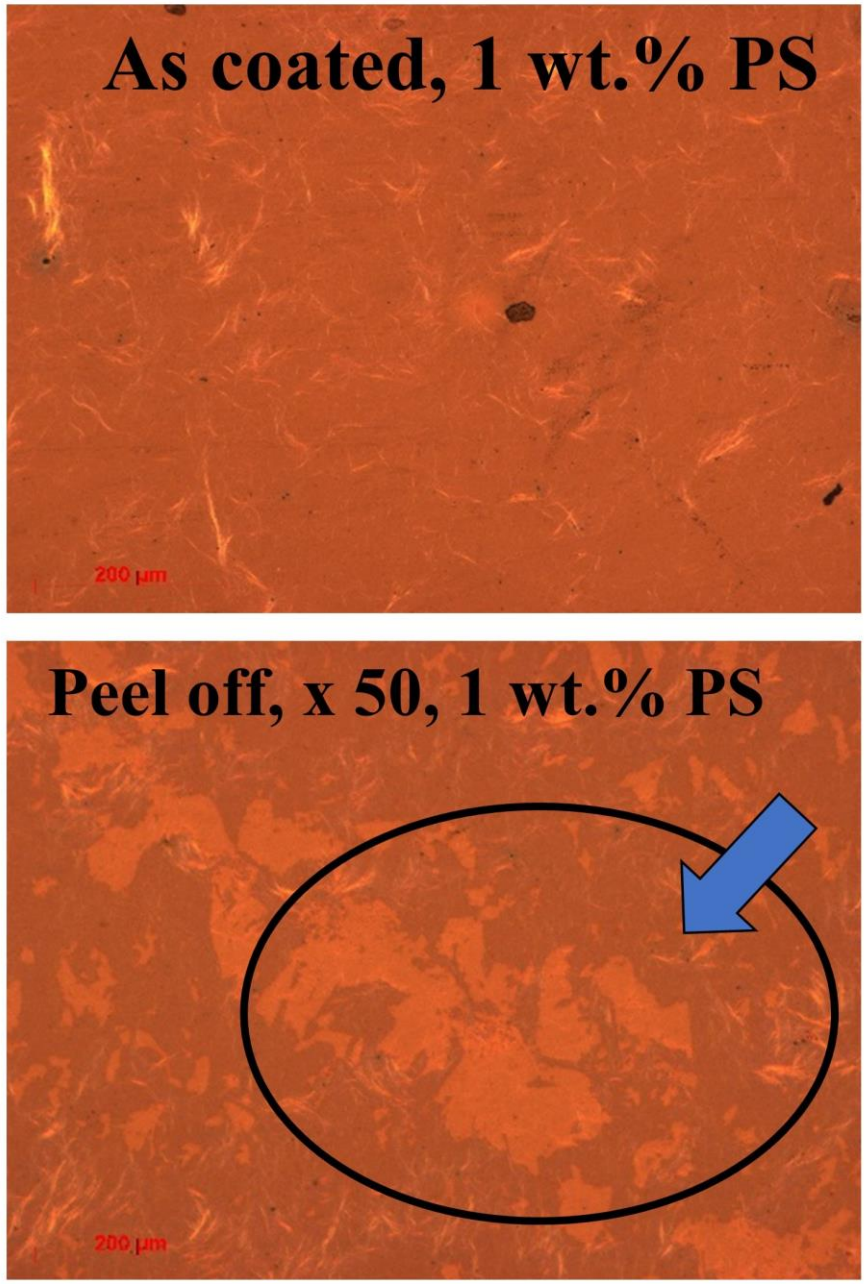

< Figure 23. Tested adhesion property of 1.0 wt.% PS (polystyrene, Mw: 100,000) >

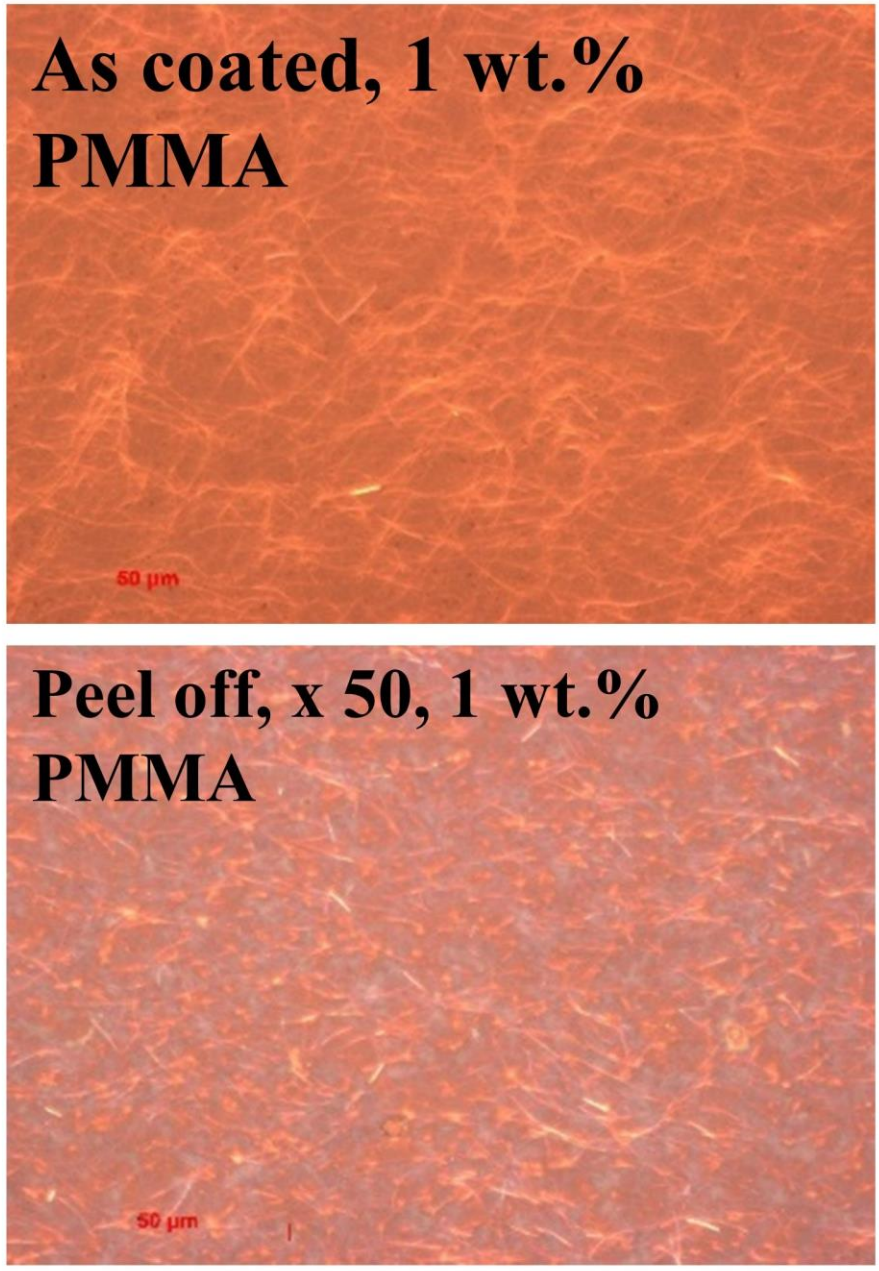

< Figure 24. Tested adhesion property of 1.0 wt.% PMMA (PMMA, Mw: 150,000) >

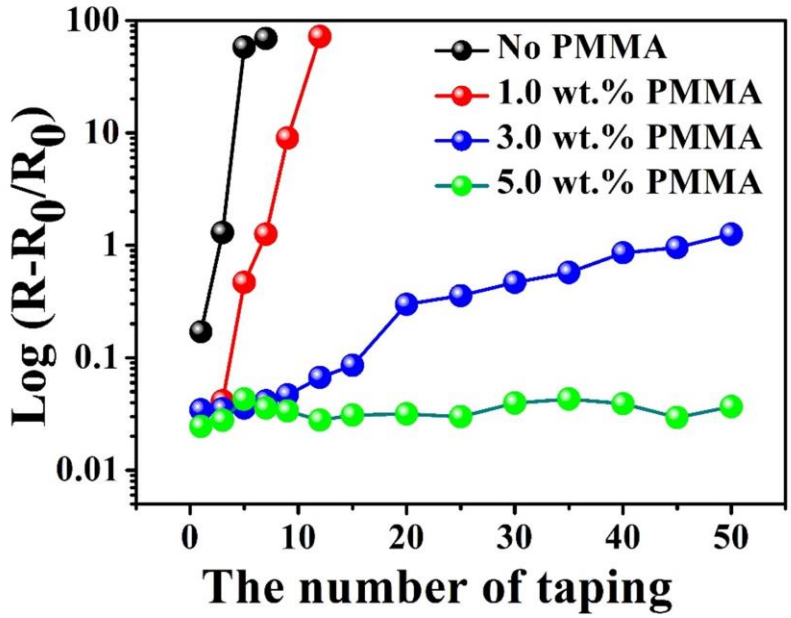

< Figure 25. Mechanical stability tests of transparent conductive PET and PES films. taping test using the Scotch tape (dark circle: unprotected PET film, red circle: 0.5 wt.% PMMA on PET film, blue circle: 1.0 wt.% PMMA on PET film, green circle: 3.0 wt.% PMMA on PET film, open red triangle: 0.5 wt.% PMMA on PES film, open blue triangle: 1.0 wt.% PMMA on PES film, open green triangle: 3.0 wt.% PMMA on PES film) >

As expected in Figure 25, the PET film with unprotected AgNWs showed a sharp increase in sheet resistance at the initial stage and no conductivity after 10 times. On the other hand, the sheet resistance of film with protected AgNWs is gradually increasing. We also found that the change depends on the PMMA content, and the higher the PMMA content, the less the resistivity change in the peel off test. We have further investigated the correlation between adhesion and surface function of films that are polyethylene terephthalate (PET) and polyether sulfone (PES). The resistance change of the PES film was slightly higher than that of the PET film. We thought that PMMA polymers had stronger interactions on the surface of the PET film.

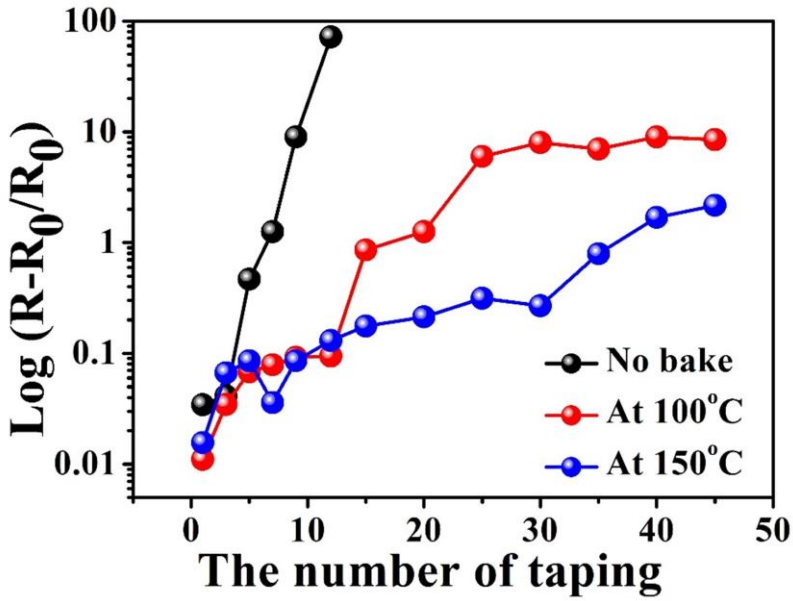

< Figure 26. Resistive changes by peel off as a function of temperature using PES film >

Additionally, conductive PES film was chosen to study the correlation between adhesion and heating effect because the glass transition temperature (T_g) of PES is higher than that of PET film in Figure 26. We baked the films for a minute at two different temperatures (100 ^oC, 150 ^oC). Then, peel test was carried out after cooling to room temperature. As a result, we have found that the adhesion property is highly dependent on bake temperature.

< Figure 27. JIBT-610, radius bending tester >

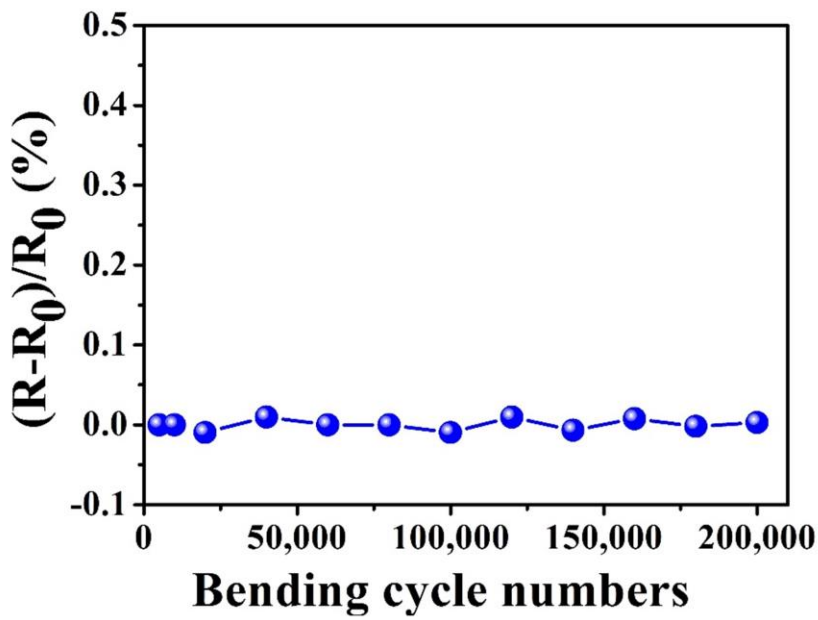

< Figure 28. Bending test (PET film): radii at 2.0 mm >

3.3.2. Thermal test

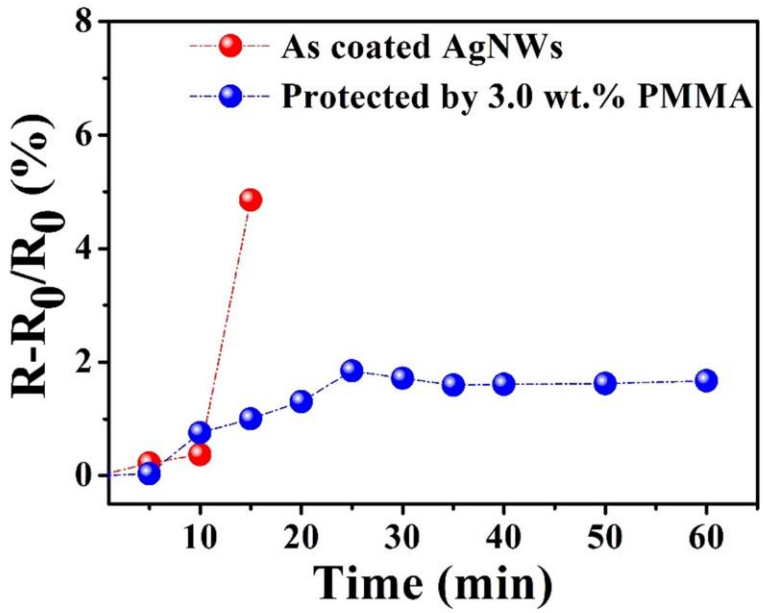

< Figure 29. Thermal durability at 200°C (PES film) for 1 hour >

We further performed bend tests and thermal stability in Figure 27, 28, and 29. The change in sheet resistance was recorded after continuous compression and deformation bending radii at 2.0 mm. We have found that the sheet resistance is stable up to 200,000 bend cycles. Interestingly, we have found that the AgNW network protected by a cross-linked PMMA polymer matrix can survive at 200 ° C and maintain electrical properties without significant change. In addition, we observed that changes in sheet resistance increased and stabilized during heating. We have assumed that the morphology of the crosslinked polymer during the initial 30 minutes affected nanowire junctions. Conversely, sheet resistance of the unprotected the AgNW network has increased significantly.

3.3.3. Surface analysis with AFM and SEM methods

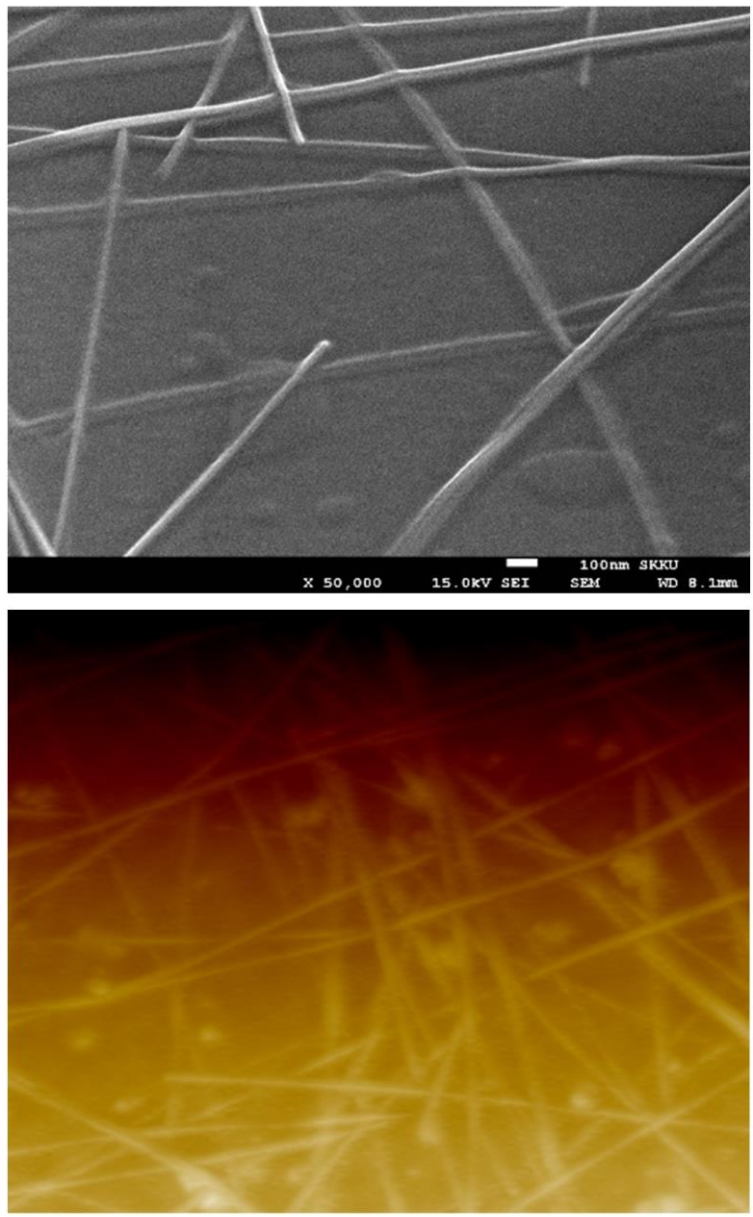

< Figure 30. Surface analysis (SEM, AFM) of AgNWs with 1.0 wt.% PMMA >

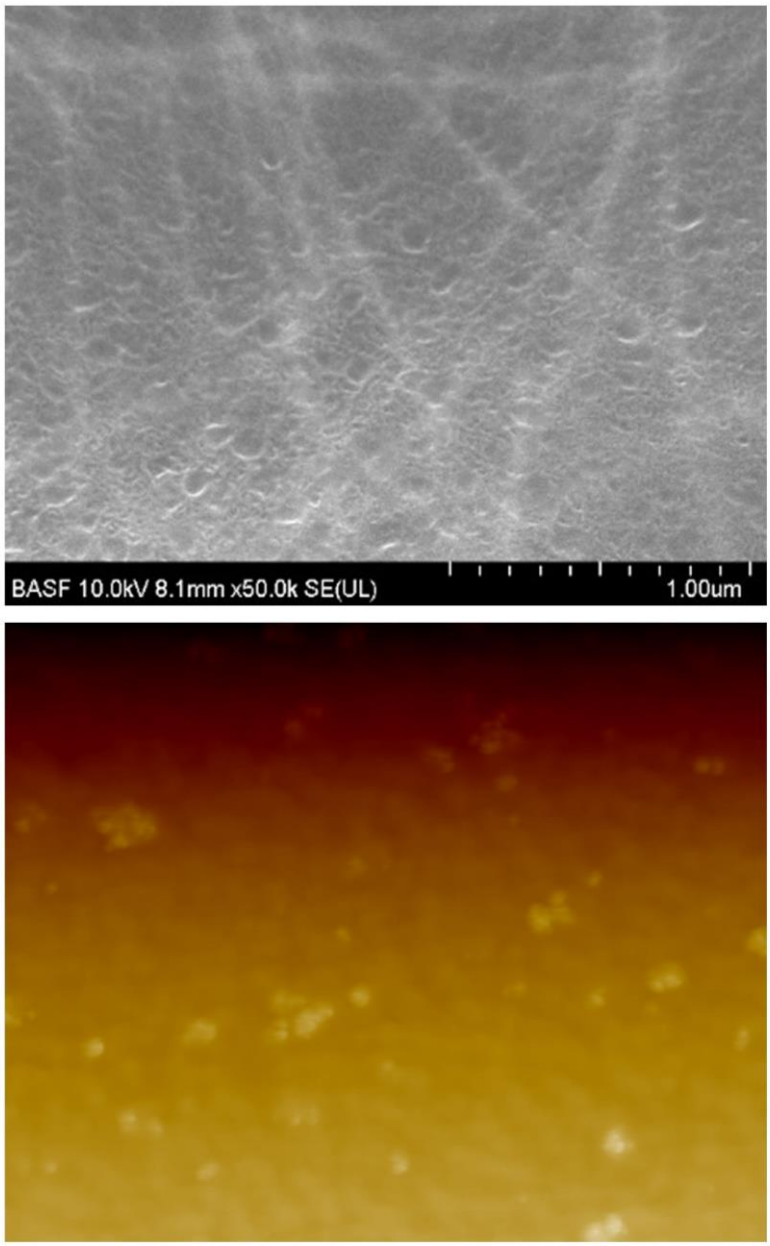

< Figure 31. Surface analysis (SEM, AFM) of AgNWs with 2.0 wt.% PMMA >

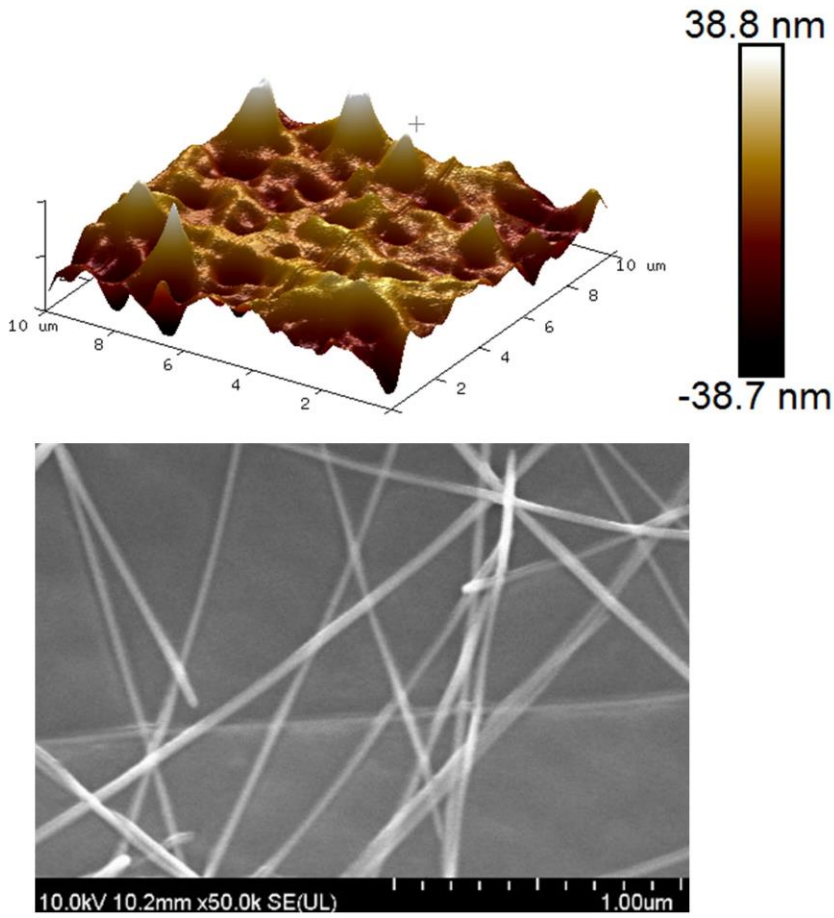

< Figure 32. 3D - Surface analysis (SEM, AFM) of AgNWs with 1.0 wt.% PMMA >

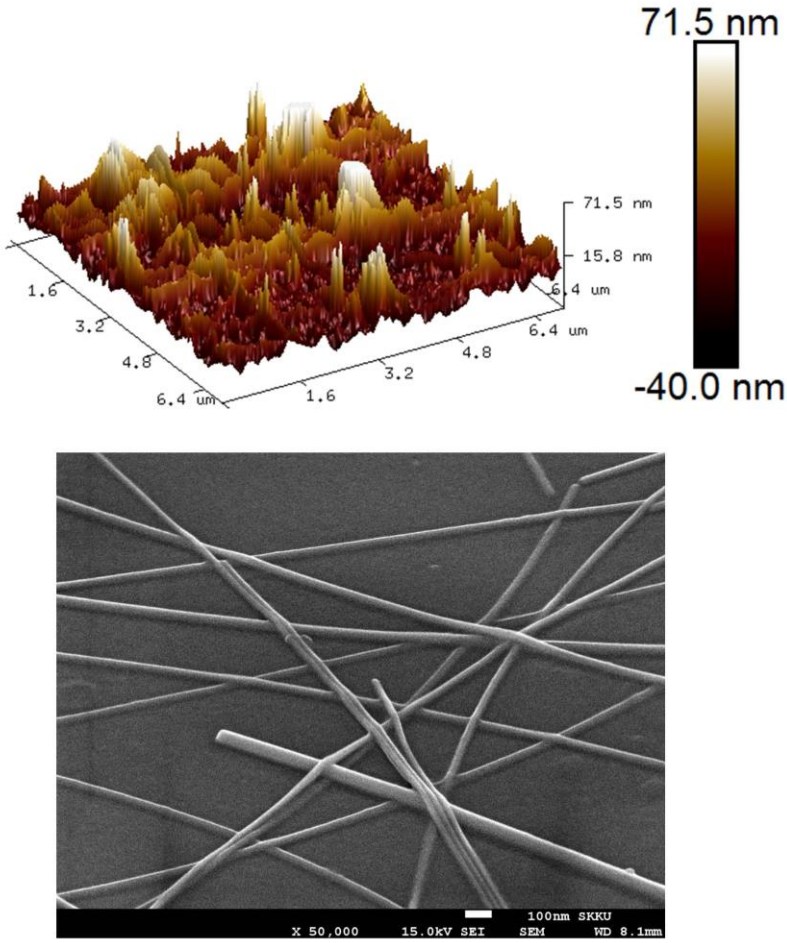

< Figure 33. 3D - Surface analysis (SEM, AFM) of AgNWs without protecion >

We have applied the developed patterning method on the organic transistor which is the core component of the future flexile electronic device. First, a simple P3HT-based organic field effect transistor (OFET) device was designed and fabricated. However, it has been observed that some transistors do not operate or exhibit significant leakage current during operation. We have assumed that there is a vertical conductivity problem in the interfacial layer between the P3HT layer and the S / D electrode. In seeking a solution, we analyzed the surface properties of AgNWs patterns protected by cross-linked PMMA.

As can be seen in Figure 30 - 33, We have found that the surface using a small amount of PMMA (1.0 wt.%) exhibits a slightly exposed AgNWs from the surface

by filling the voids of the AgNW network. On the other hand, the high content of PMMA (2.0 wt.%) covered the entire AgNW network. We further performed atomic force microscopy (AFM) and scanning electron microscopy (SEM) analysis to confirm the RMS roughness value of the surface using 1.0 wt.% PMMA polymer and compared it with the unprotected AgNW network in Figure 32 and 33. The RMS roughness value of the AgNW network using 1.0 wt.% PMMA was about 8 nm and the peak to valley value was 35 nm when compared to the unprotected AgNW network (RMS: > 13 nm, Rpv > 70 nm). As a result, our approach controlling surface roughness is simply to adjust the polymer content. We compared the values of AgNWs-polymer composite known from the literature, and confirmed that the results have similar RMS values.

3.4. Applications

3.4.1. Film type electrical connectors

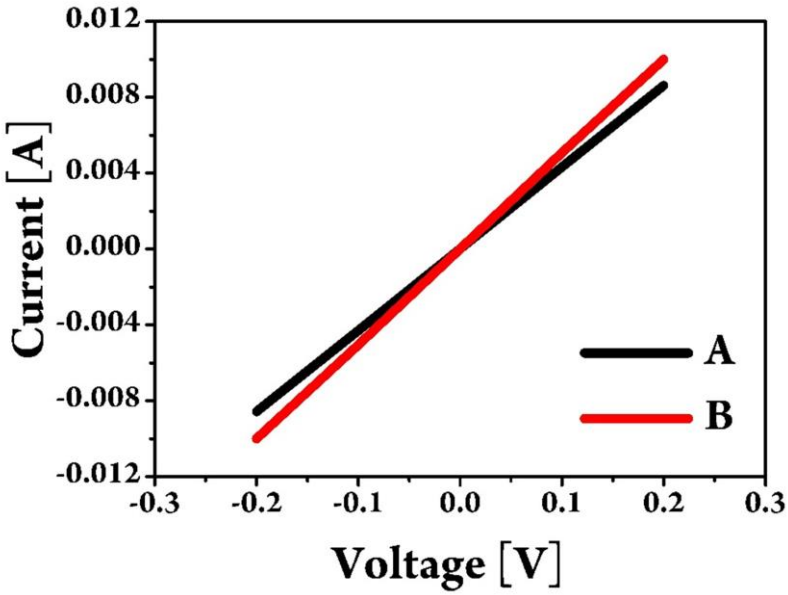

< Figure 34. Line widths dependent electrical property >

For electrodes, confirmation of resistance changes as a function of line width is very important. Therefore, we selected two line widths – 50 μm and 25 μm, and silver metal was deposited on the patterned lines through thermal evaporation method for accuracy of probing of randomly deposited AgNW networks. As can be seen Figure 34, the electrical resistance changes of two line widths were recorded. We confirmed that the 50 μm line width exhibited slightly better current flows compared to 25 μm patterns.

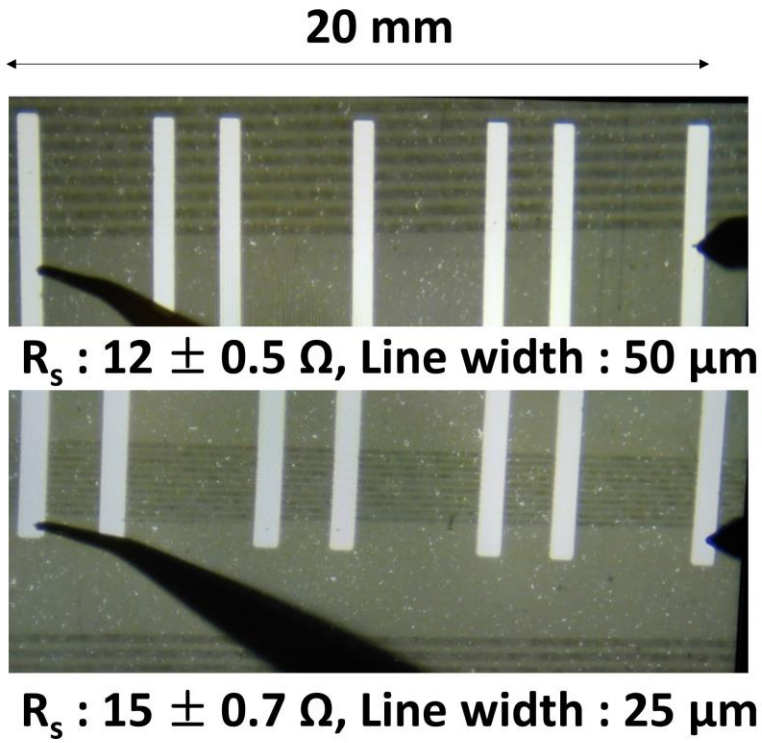

< Figure 35. Distance dependent resistivity property >

Likewise, we have also tested resistance changes as a function of distance. The resistance value of 25 μm patterns as an example is increased as a function of distance. These resistance changes at the different line widths could be resulted from due to the difference in the number of percolating junctions in the finely patterned lines. We think that these changes of resistance depending on patterned line widths could be improved by increasing the number of nanowires like previous suggestion.

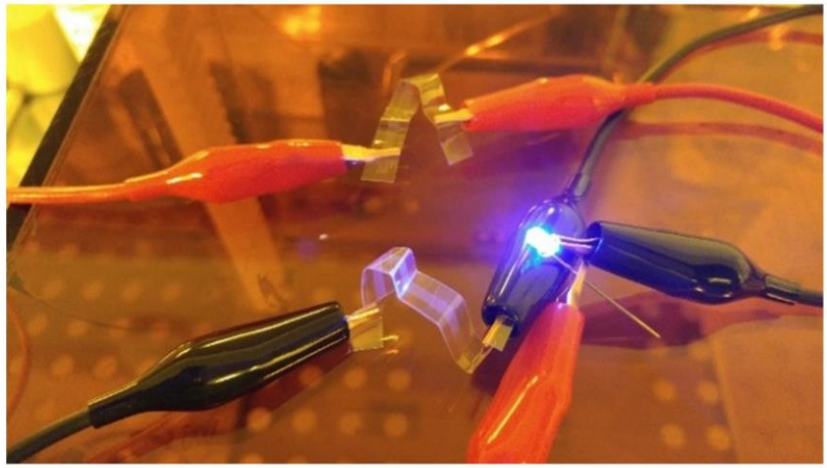

< Figure 36. Applications: film type electrical connector >

For applications of our patterning methods, we prepared a finely patterned transparent conductive film in Figure 36. It was then utilized for film type electrical connectors to turn on LEDs. The film was bent and crumbled several times to confirm mechanical stability of protected AgNW networks. It turned out that the protected AgNWs exhibited excellent electrical conductivity and mechanical stability for continuous deformations.

3.4.2. Source / Drains for P3HT Organic FETs

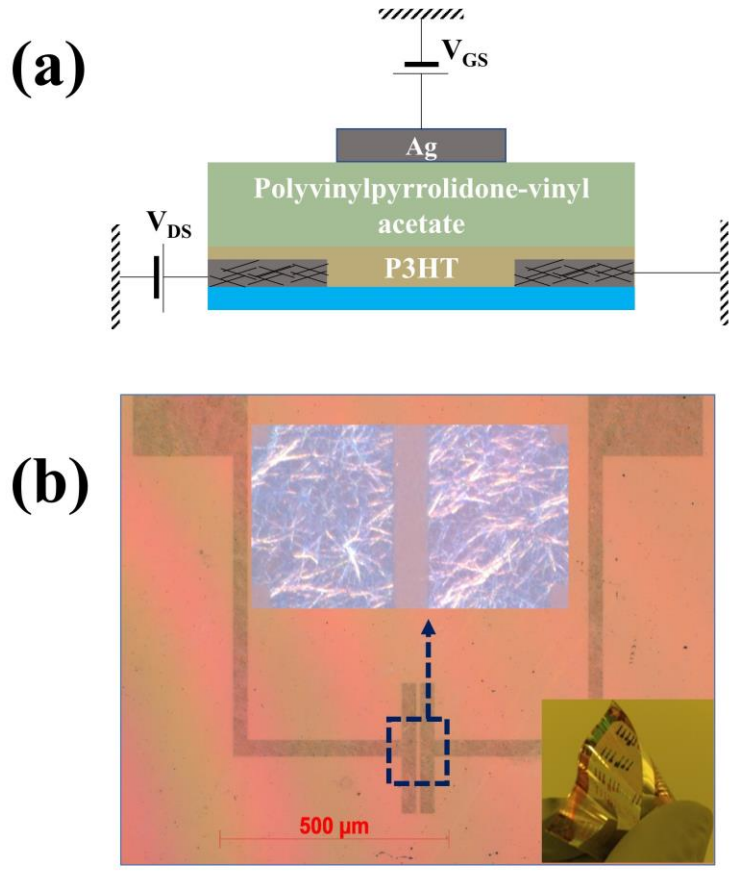

< Figure 37. Applications: an illustration of fabricated device, organic P3HT transistor using AgNWs as source and drain electrode, (the inset is a prepared OFET device) >

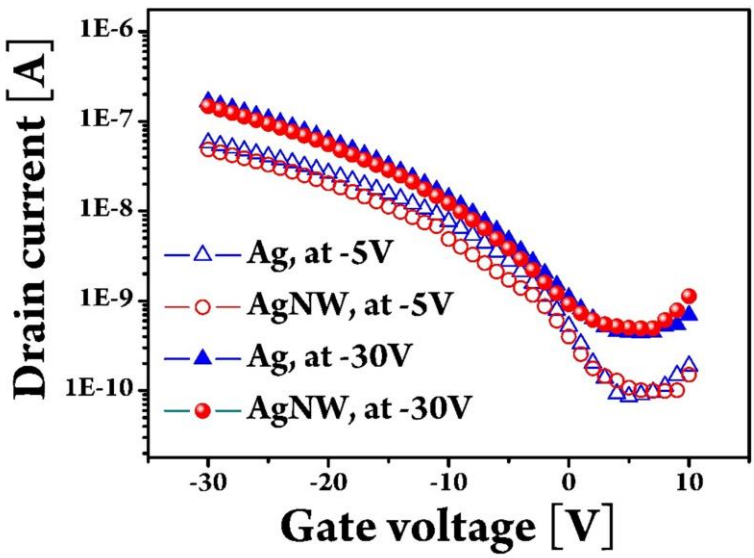

< Figure 38. Transfer curve behavior of organic P3HT transistor using AgNWs as source and drain electrode, channel lengths and line widths are 10 μm and 250 μm >

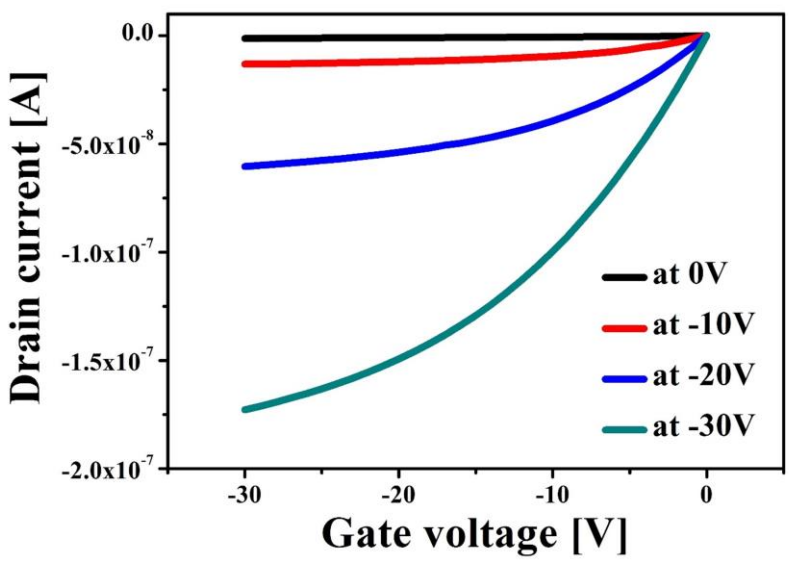

< Figure 39. output curve of transistor with AgNWs as S/D electrodes >

Based on the surface optimizations, we re-fabricated a P3HT-based OFET device with source (S) / (D) drain electrodes patterned with channel lengths and line widths of 10 μm and 250 μm, respectively, in Figure 37. The transfer curves of P3HT OFET produced by the patterned AgNWs S / D electrodes were compared to a typical P3HT OFET with evaporated silver metal in Figure 38 and 39. The output curves for the AgNWs S / D electrodes are shown in Figure 36. As a result, we confirmed that a P3HT-based organic transistor using AgNWs is almost equivalent to a P3HT organic transistor based on a metal S / D electrode.

Chapter 4. Dispersion of QDs and Photolithographic Patterning

4.1. QDs dispersion in the polar media

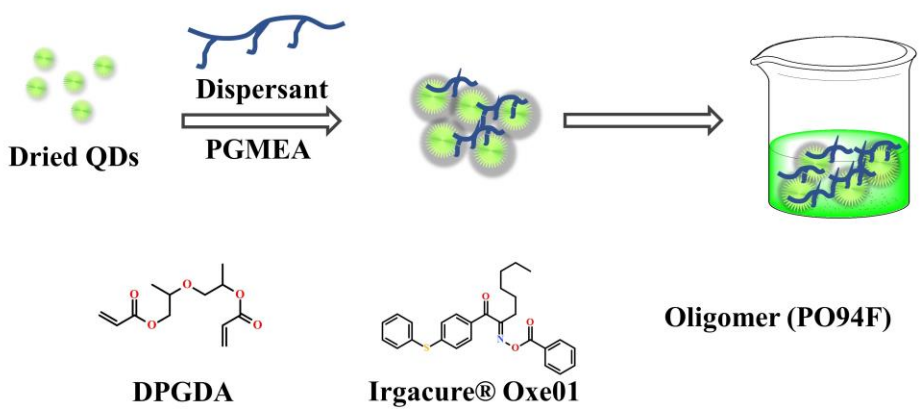

< Figure 40. Illustrations for preparation of photosensitive QD compositions, blending method with commercial materials, oligomer (PO94F), BASF SE >

In this study, non-polar ligand-capped CdSe/ZnS core/shell QDs without surface modifications was used. Figure 40 shows the overall illustration of blending methods and the prepared QD compositions at high loading concentrations (30 wt.%) in PGMEA, which is one of the most popular solvents in industry. Commonly, prepared QDs are re-dispersed in non-polar solvents (Toluene, or Hexane) for transport and storage. However, these impractical solvents must be replaced by less toxic solvents such as propylene glycol monomethyl ether acetate (PGMEA) for practical application in industry.

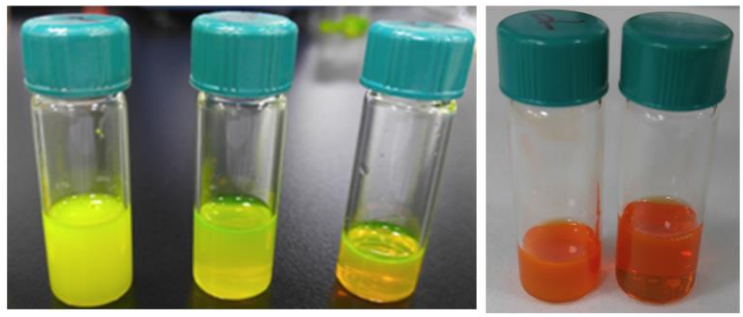

< Figure 41. Illustrations dispersion tests: (b-1) without using dispersants, (b-2) DisperBYK-163, (b-3) DisperBYK-180, (b-4) DisperBYK-163 with red QDs, (b-5) DisperBYK-180 with red QDs >

As a first step, we considered whether it could rule out the solvent exchange step. Instead of re-dispersing in a non-polar solvent to avoid the solvent exchange step, the prepared QD was dried in vacuum for 3 hours. Through experimentation, we figured out that the quantum yield and optical properties are stable. Moreover, the dried QDs can be stored in the air for several weeks. Then, we attempted to disperse as dried QDs into a mixture of PGMEA and hydrophilic binders (polyether acrylate oligomers with high acid value, 230 mg KOH / g, BASF). However, we observed that the blends were easily turbid and eventually formed sediments in Figure 41, (b-1). Due to incompatibility, we had to find suitable dispersants. We have found that there are many dispersants used for dispersing nanoparticles in the painting and coating industry. We searched for block copolymers with different acid values (referred to as “mg KOH / g”), which serve as high molecular weight wetting and dispersing agent for solvent-borne systems. Our study has been started from two commercial dispersants: (i) DisperBYK - 163 (10 mg KOH / g), (ii) DisperBYK - 180 (94 mg KOH / g), which can trigger deflocculating through steric stabilization of QDs.

30 wt.% QD blends

< Figure 42. Illustrations for prepared 30 wt.% QD compositions >

To evaluate dispersibility, we conducted blending tests at lower QD concentrations (10 wt.% of QDs). Figure 39, (b-2), (b-3), (b-4), and (b-5) shows the results of the dispersed QDs in different dispersants. We confirmed that higher acid numbers can disperse QDs more efficiently. However, we still observed that the blends became turbid and formed sediments in a few minute. Then, we further added oligomeric binders having high acid values (PO94F, 230 mg KOH / g), which is polyether acrylates, into the QD blends with DisperBYK - 180. Then, we found polyether acrylate type oligomer can successfully disperse turbid QD blends. Based on the results, we think that the deflocculated QD particles by steric stabilizations in PGMEA might be further agglomerated in oligomeric binders. Eventually, the blend with DisperBYK - 180 and oligomeric binders was mixed with the prepared cocktails comprised of extra oligomeric binders, cross-linkable monomers (dipropylene glycol diacrylate, DPGDA), and oxime ester photoinitiators (Irgacure® Oxe01, BASF) in PGMEA (see Experiment). Fortunately, we did not experience any difficulties during this step. Therefore, we tried to prepare higher concentration of QD blends up to 30 wt. % in the same way. Figure 42 shows the uniformly dispersed high concentration of QD blends. We concluded that our methods can produce high concentration of QD blends in an efficient way without solvent exchange step and additional surface modifications.

4.2. PL Changes During QD Blending

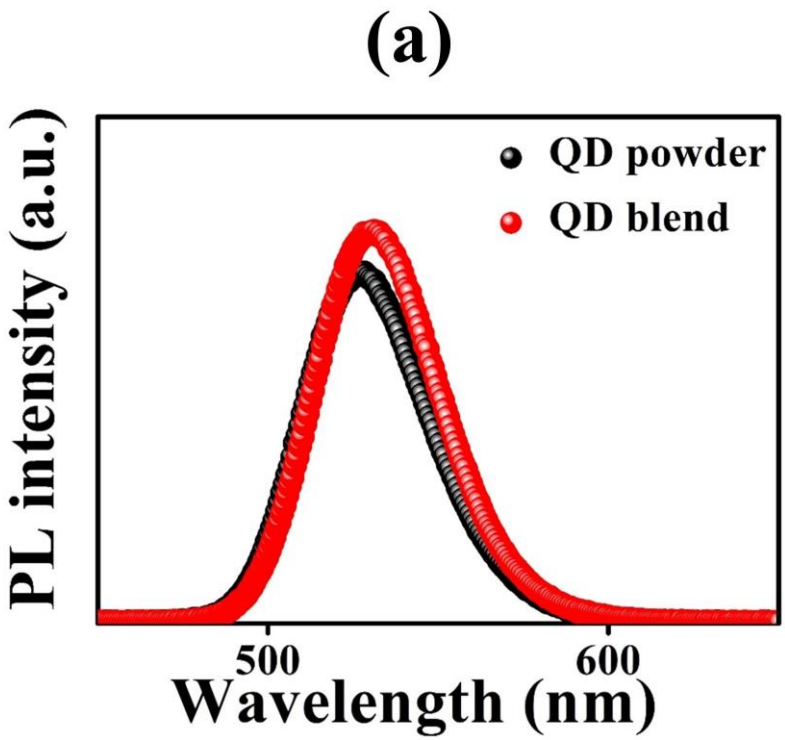

< Figure 43. The photoluminescence (PL) properties before and after blending, green QD blends having a 523 nm peak emission wavelength >

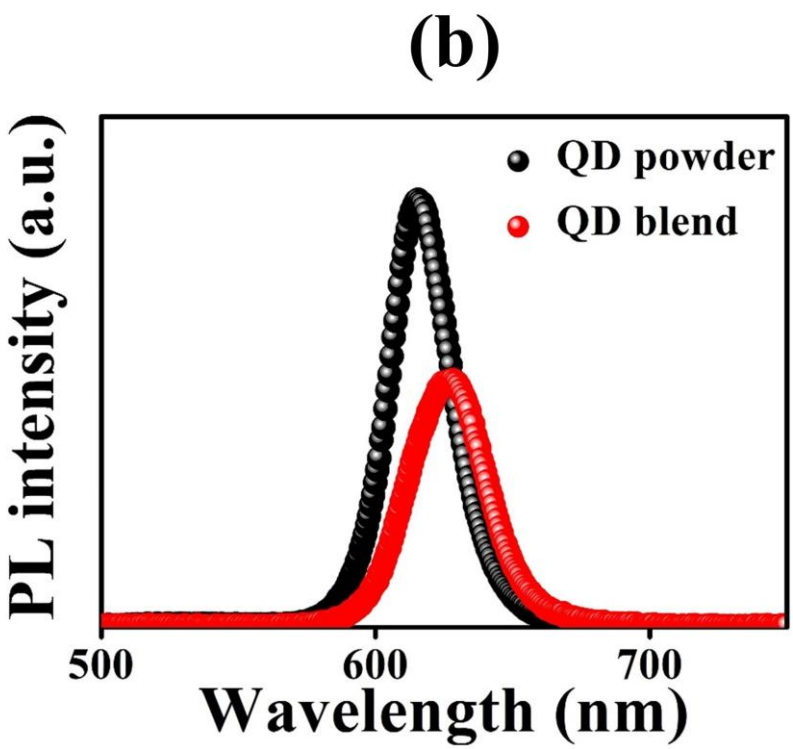

< Figure 44. The photoluminescence (PL) properties before and after blending, red QD blends having a 616 nm peak emission wavelength >

To evaluate the optical properties before and after blending, we analyzed the PL emission property and photoluminescence quantum yields (PLQYs) of QD blends. The PL emission spectrum of CdSe@ZnS compositions having peak emission wavelengths of 523 nm and 616 nm, respectively, is shown in Figure 43, 44. For both QD compositions, the PL emission spectrum generally has the same shape but exhibits a slight bathochromic shift of the emission spectrum. For the PL intensity, the CdSe@ZnS compositions with a peak emission wavelength of 523 nm showed slightly increased intensity [57, 58], but the CdSe@ZnS compositions a peak emission wavelength of 616 nm exhibited a significant reduction in PL intensity, indicating PL quenching. We can infer, but have not proven, that a significant reduction in PL intensity and PLQYs is primarily due to trapping on surface [59], ligand induced spectral changes [60, 61] and ligand degradation during physical blending [62].

4.3. PL Changes During UV Curing / Baking

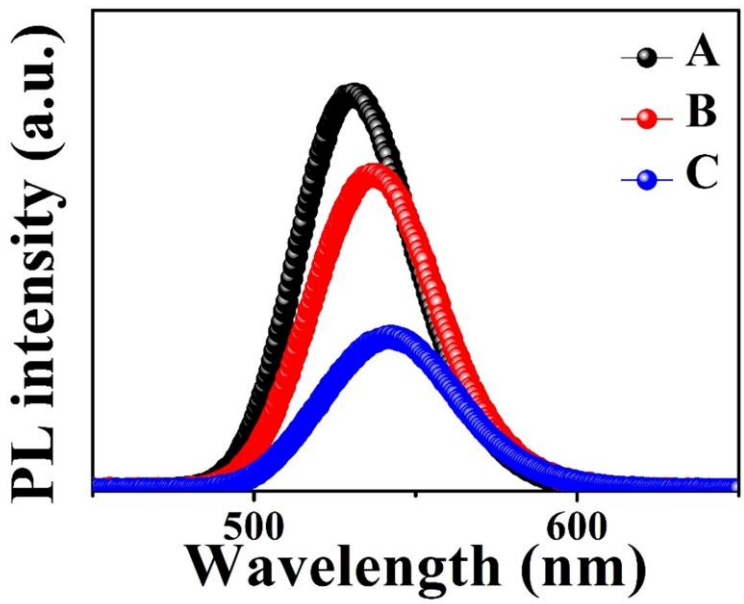

< Figure 45. The PL spectrum changes during the patterning process, green QD compositions, A: pre-baking step (100°C) on a hot plate, B: UV exposure (i-line), C: post-baking step (180°C) on a hot plate >

Subsequently, to verify quantum efficiency and optical properties during the patterning process, a QD film was prepared using a composition having 20 wt.% of QDs according to the spin coating method and the following process: (A) pre-baking at 100 °C for 1 minute, (B) UV exposure, and (C) post-baking at 180 °C for 30 minutes.

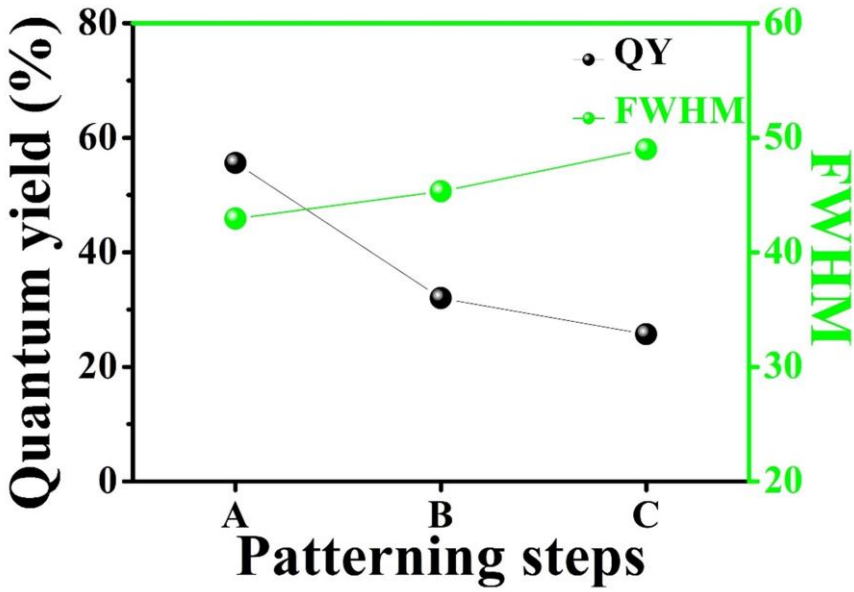

< Figure 46. The PLQYs, and FWHMs changes during the patterning process, green QD compositions, A: pre-baking step (100^{o}C) on a hot plate, B: UV exposure (i-line), C: post-baking step (180^{o}C) on a hot plate >

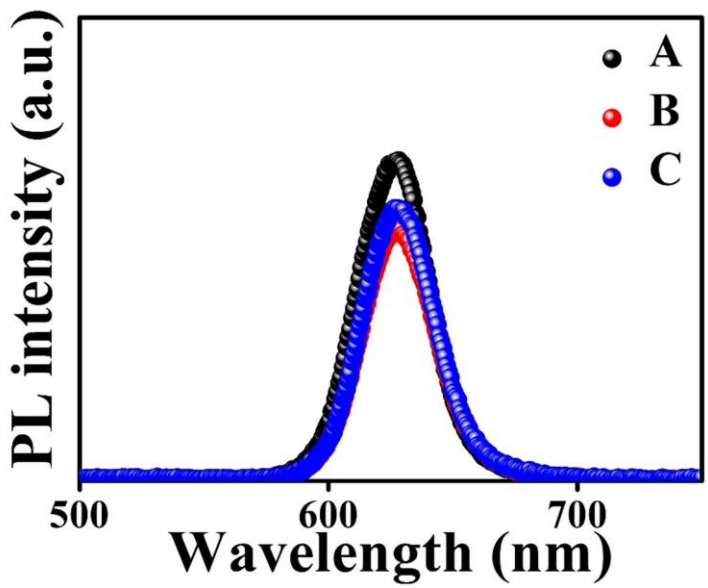

< Figure 47. The PL spectrum changes during the patterning process, red QD compositions, A: pre-baking step (100^{o}C) on a hot plate, B: UV exposure (i-line), C: post-baking step (180^{o}C) on a hot plate >

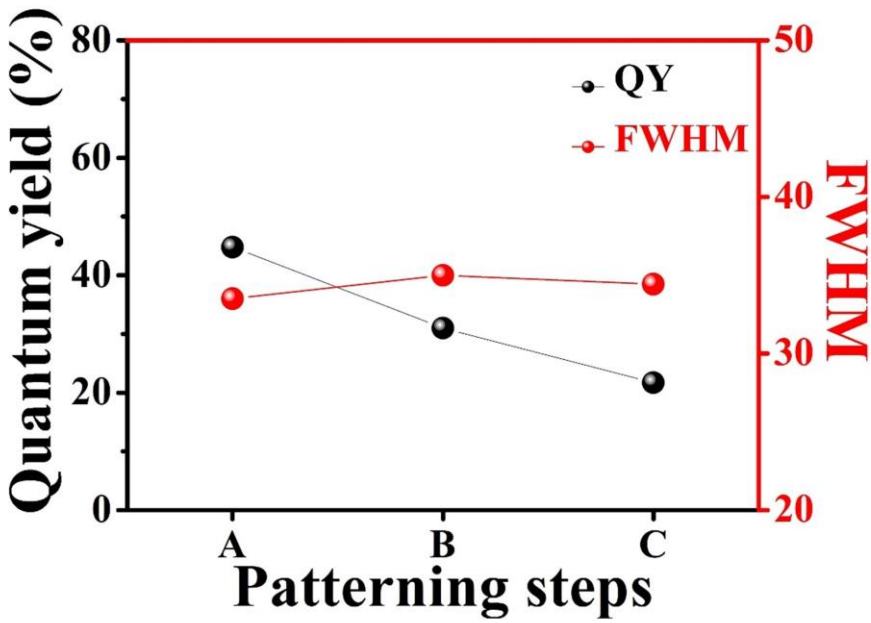

< Figure 48. The PLQYs, and FWHMs changes during the patterning process, red QD compositions, A: pre-baking step (100^{o}C) on a hot plate, B: UV exposure (i-line), C: post-baking step (180^{o}C) on a hot plate >

Figure from 45 to 48 shows the photoluminescence properties and the changes in PLQYs of both QD films during the photolithography process. The PLQYs of the green QD film was reduced by 20.3 % from 56 % (A) to 25.7 % (C) in Figure 46, and the PL spectra showed significant bathochromic shifts of the emission spectrum with a much wider full width at half maximum (FWHM). We believe that the intensity reduction and bathochromic shift of PL spectrum might be originated from QDs aggregation during polymerization and thermal degradation in air during the process. On the contrary, red QD films showed less deterioration in PLQYs (reduced by 13.3 %, from 45 % (A) to 21.7 % (C) with retained the PL spectrum and FWHM overall in Figure 48.

4.4. Fine Patterning

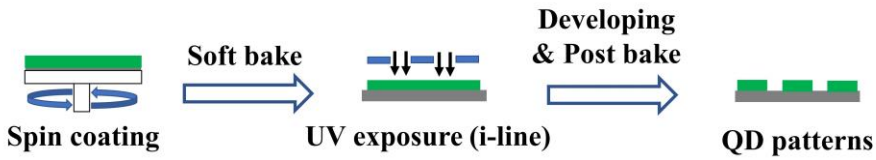

< Figure 49. Illustrations for photolithographic patterning QD compositions >

We varied the weight ratio of QDs in the compositions (20 wt.% and 30 wt.%, respectively). It shows various QD patterns at high concentration of QDs (20 wt.% vs 30 wt.%). QD compositions that are capable of photolithographic patterning were spin coated on glass in Figure 49.

The coated QD layer was baked at 100 ^{o}C to evaporate excess solvent and exposed to UV-light (i-line) with a photo-mask for 2 seconds. For efficient and fast developing conditions, we examined two methods: PGMEA alone and basic TMAH (tetrahydromethylammonium hydroxide) solution (0.2 wt.% in water). We have found that both methods can efficiently develop and form QD images within 30 seconds. However, we observed many defects on the surface of QD images and physically delaminated QDs images when the basic TMAH solution was applied for developing. On the contrary, the only PGMEA did not show any defects and delaminated QD images. Based on the results, we can deduce that the used UV curable polymeric matrix has good resistance to PGMEA. Finally, the developed QD image was further baked (called post-baking) at 180 ^{o}C for 30 minutes.

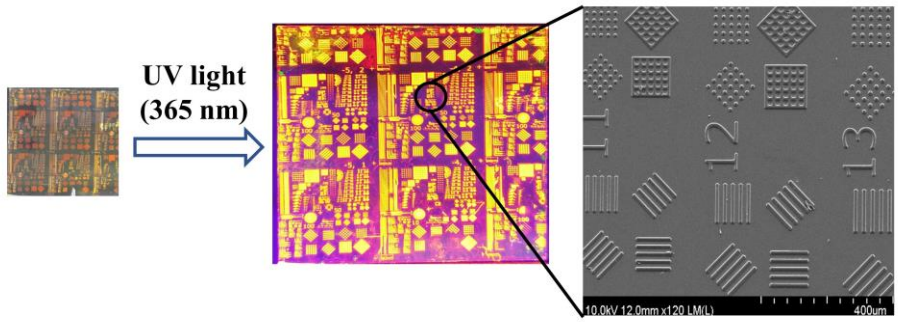

< Figure 50. Demonstration of 20 wt.% QD compositions and various images of QD patterns by SEM analysis >

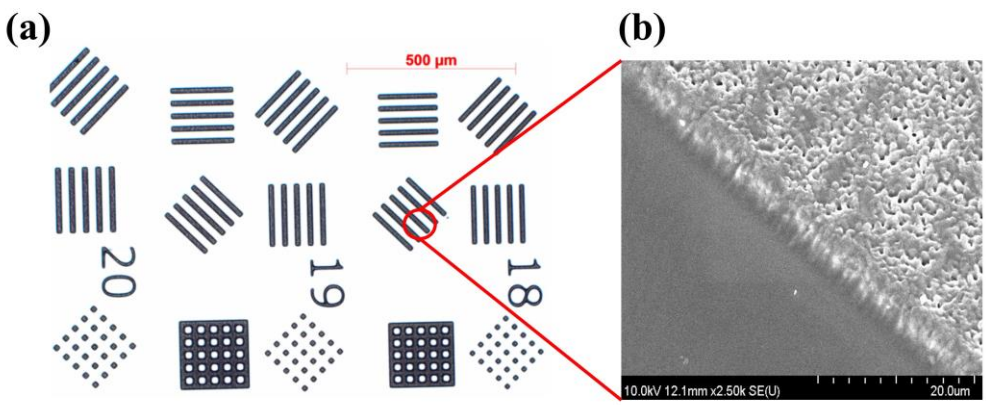

< Figure 51. Demonstration of 30 wt.% QD compositions and various images of QD patterns by SEM analysis >

The pattern images (6 μm thickness in average) were further confirmed by SEM in Figure 50. It turned out that any aggregates and surface defects on the patterned QDs image are not observed. On the other hands, the QDs image in Figure 51 produced by the increased QDs content (30 wt.%) have many pinhole-like surface defects on the patterned image, indicating some difficulty of fine patterning at higher QD concentrations due to interrupting cross-linking, trapping radicals on QD surface, but have not been proven.

Chapter 5. Conclusion

In summary, we have developed an etchant-free AgNWs patterning method. We have found that ultra-sonication processing can be used for fine AgNWs patterning using conventional photolithography processes. We have made transparent fine patterns with clear line edges up to 20 μm without the use of photoresist, wet chemical etchants. We have also found that AgNWs protected by a polymer matrix has excellent mechanical stability. During taping and bending tests, no significant increase in sheet resistance was seen during up to 200,000 bending cycles. We have also found that AgNWs, which are protected by cross-linking the PMMA matrix, maintain electrical stability at 200 ^{o}C for 1 hour. Finally, our patterning method was applied to the S / D electrode of a P3HT-based organic field effect transistor and confirmed to be approximately the same as a transistor using a deposited silver metal. We believe that this method can provide an alternative way to other applications where it is necessary to avoid corrosive wet chemical etching solutions. We are further optimizing the techniques for many patterning applications for flexible optoelectronics.

For QDs as another type of nanomaterial, we demonstrated QD blending with high loading QDs (up to 30 wt.%), which is capable of photolithographic patterning. We have proposed efficient blending methods for photosensitive QD compositions by varying the amount of QDs. We have shown that our blending method is not required for additional time-consuming processes such as solvent exchange, surface modifications of hydrophobic QDs. For uniform QD blending in a polar solvent (PGMEA), we have proposed commercially viable dispersants, hydrophilic oligomeric binders, and other additives. We evaluated PLQYs and optical properties retention during the QD film process. However, we have observed that

there are significant deteriorations due to some reasons, which are under investigations and further optimizations. Finally, we have demonstrated finely patterned QD images with a less than 20 m width and 6 m thickness by using conventional photolithographic patterning method. High concentrations of QD blends up to 20 wt.% were successfully patterned without any difficulties such as pinhole-like surface defects and physical de-laminations during the developing in photolithography process. Based on our work, many research communities hope to join in this field intensively in the near future.

Bibilography

[1] Jingjing Ma, Maosheng Zhan, RSC Advances, 40, 2014, 21060 (2014)

[2] S. De, T. M. Higgins, P. E. Lyons, E. M. Doherty, P. N. Nirmalraj, W. J. Blau, J. J. Boland, and J. N. Coleman, *Acs Nano* 3, 1767 (2009).

[3] A. Kumar and C. W. Zhou, *Acs Nano* 4, 11 (2010).

[4] L. B. Hu, H. S. Kim, J. Y. Lee, P. Peumans, and Y. Cui, *Acs Nano* 4, 2955 (2010).

[5] E. Amini, M. Dolatyari, A. Rostami, H. Shekari, H. Baghban, H. Rasooli, and S. Miri, *IPTL* 24, 1995 (2012).

[6] Y. J. Wang, T. Feng, K. Wang, M. Qian, Y. W. Chen, and Z. Sun, *Journal of Nanomaterials* 935218 (2011).

[7] A. R. Madaria, A. Kumar, F. N. Ishikawa, and C. W. Zhou, *Nano Research* 3, 564 (2010).

[8] C. H. Liu and X. Yu, *Nanoscale Research Letters* 6, (2011).

[9] J. Y. Lee, S. T. Connor, Y. Cui, and P. Peumans, *Nano Lett*. 10, 1276 (2010).

[10] T. Kim, A. Canlier, G. H. Kim, J. Choi, M. Park, and S. M. Han, *Acs Applied Materials Interfaces* 5, 788 (2013).

[11] T. Kim, Y. W. Kim, H. S. Lee, H. Kim, W. S. Yang, and K. S. Suh, *Adv. Funct. Mater.* 23, 1250 (2013).

[12] J. V. van de Groep, P. Spinelli, and A. Polman, *Nano Lett.* 12, 3138 (2012).

[13] J. Lim, W. Bae, J. Kwak, S. Lee, C. Lee, and K. Char. Optic. Mater. Exp, 2, 594 (2012)

[14] P. Reiss, M. Carriere, C. Lincheneau, L. Vaure, and S. Tamang et al., Chem. Rev, 116, 10731 (2016)

[15] J.M. Pietryga, Y.S. Park, J. Lim, A.F. Fidler, W.K. Bae, S. Brovelli, and V. I. Klimmov, Chem. Rev, 116, 10513 (2016)

[16] W.K. Bae, M. K Nam, K. Char, and S. Lee, Chem. Mater, 20, 5307 (2008)

[17] W. K. Bae, K. Char, H. Hur, S. Lee, 20, 531 (2008)

[18] C. M. Donega, S. G. Hickey, S. F. Wuister, D. Vanmaekelbergh, A. Meijerink, J. Phys. Chem. B, 107, 489 (2003)

[19] C. B. Murray, D.J. Norris, and M. G. Bawendi, J. Am. Chem. Soc, 115, 8706 (1993)

[20] Dmitry Aldakov. A. Lefrancois, and P. Reiss, J. Mater. Chem. C, 1, 3756 (2013)

[21] Raul Calzada.; Christopher M. Thompson.; Dana E. Westmoreland.; Kedy Edme.; Emily A. Weiss. *Chem. Mater*. 2016, 28, 6716−6723.

[22] Heidi R. Culver.; Stephanie D. Steichen.; Margarita Herrera-Alonso.; Nicholas A. Peppas. *Langmuir* 2016, 32, 5629−5636.

[23] Kim De Nolf.; Salvatore M. Cosseddu.; Jacek J. Jasieniak.; Emile Drijvers.; José C. Martins.; Ivan Infante.; Zeger Hens. *J. Am. Chem. Soc*. 2017, 139, 3456−3464.

[24] Fabien Dubois.; Benoıˆt Mahler.; Benoıˆt Dubertret.; Eric Doris.; Charles Mioskowski. *J. Am. Chem. Soc*. 2007, 129, 482-483.

[25] Junsheng Chen.; Bin Yang.; Chuanshuai Li.; Kaibo Zheng.; Karel Žídek.; Tõnu Pullerits. *ACS Omega.* 2017, 2, 1922−1929.

[26] Zhi-Liang Chen.; Yi Lin.; Xiao-Juan.; Dong-Liang Zhu.; San-Wei Guo.; Jing-Jing Zhang.; Jia-Jia Wang.; Bao-Shan Wang.; Zhi-Ling Zhang.; Dai-Wen Pang. *ACS Appl. Mater. Interfaces*, 2017, 9, 39901-39906.

[27] Yu Yang, Haiyan Qin.; Maowei Jiang.; Long Lin.; Tao Fu.; Xingliang Dai.; Zhenxing Zhang.; Yuan Niu.; Hujia Cao.; Yizheng Jin.; Fei Zhao.; Xiaogang Peng. *Nano Lett*, 2016, 16, 2133−2138.

[28] Goutam Palui.; Tommaso Avellini.; Naiqian Zhan.; Feng Pan.; David Gray.; Igor Alabugin.; Hedi Mattoussi. *J. Am. Chem. Soc*, 2012, 134, 16370−16378.

[29] Wenzhuo Guo.; J. Jack Li.; Y. Andrew Wang.; Xiaogang Peng. *J. Am. Chem. Soc*. 2003, 125, 3901-3909.

[30] Cai-Feng Wang.; Fengjia Fan.; Randy P. Sabatini.; Oleksandr Voznyy.; Kristopher Bicanic.; Xiyan Li.; Daniel P. Sellan.; Mayuran Saravanapavanantham.; Nadir Hossain.; Kefan Chen.; Sjoerd Hoogland.; Edward H. Sargent. *Chem. Mater*, 2017, 29, 5104-5112.

[31] Matthew A. Koc.; Shilpa N. Raja.; Lindsey A. Hanson.; Son C. Nguyen.; Nicholas J. Borys.; Alexander S. Powers.; Siva Wu.; Kaori Takano.; Joseph K. Swabeck.; Jacob H. Olshansky.; Liwei Lin.; Robert O. Ritchie.; A. Paul Alivisatos. *ACS Nano*, 2017, 11, 2075–2084.

[32] Marcus J. Smith.; Sidney T. Malak.; Jaehan Jung.; Young Jun Yoon.; Chun

Hao Lin.; Sunghan Kim.; Kyung Min Lee.; Ruilong Ma.; Timothy J. White.; Timothy J. Bunning.; Zhiqun Lin.; Vladimir V. Tsukruk. Robust, *ACS Appl. Mater. Interfaces*, 2017, 9, 17435−17448.

[33] Chao Liu.; Zhou Li.; Tibor Jacob Hajagos.; David Kishpaugh.; Dustin Yuan Chen.; Qibing Pei. *ACS Nano*, 2017, 11, 6422−6430.

[34] Jun Wang, Jinting Jiu, Tohru Sugahara, Shijo Nagao, Masaya Nogi, Hirotaka Koga, Peng He, Katsuaki Suganuma, Hiroshi Uchida, ACS Appl. Mater. Interfaces, 7 (2015), 23297-23304.

[35] Dabum Kim, Youngsang Ko, Wooki Kim, Donghyuk Kim, Jungmok You, Opt. Mater. Express, 7 (2017), 2272-2279.

[36] Youngsang Ko, Jeonghun Kim, Dabum Kim, Yusuke Yamauchi, Jung Ho Kim, Jungmok You, Sci. Rep, 2017, DOI:10.1038/s41598-017-02511-8.

[37] Anuj R. Madaria, Akshay Kumar, Fumiaki N. Ishikawa, Chongwu Zhou, Nano Res, 3 (2010), 564-573.

[38] Chang-Hyun Song, Ki-Hoon Ok, Chan-Jae Lee, Youngmin Kim, Min-Gi Kwak, Chun Jong Han, Namsu Kim, Byeong-Kwon Ju, Jong-Woong Kim, Org. Electron, 17 (2015), 208 – 215.

[39] Harim Oh, Jeeyoung Lee, Jin-Hoon Kim, Jin-Woo Park, Myeongkyu Lee, J. Phys. Chem. C, 120 (2016), 20471 - 20477.

[40] Gui-Cang He, Mei-Ling Zheng, Xian-Zi Dong, Feng Jin, Jie Liu, Xuan-Ming Duan, Zhen-Sheng Zhao, Sci. Rep, 7 (2017), 41757-

[41] William J. Scheideler, Jeremy Smith, Igal Deckman, Seungjun Chung, Ana Claudia Arias, Vivek Subramanian, J. Mater. Chem. C, 4 (2016), 3248 - 3255.

[42] Jong Deck Park, Sooman Lim, Haekyoung Kim, Thin Solid Films, 586 (2015), 70-75.

[43] Hui Lu, Jian Lin, Na Wu, Shuhong Nie, Qun LuO, Chang-Qi Ma, Zheng Cui, Appl. Phys. Lett, 106 (2015), 093302.

[44] Hyungseok Kang, Iljoong Kang, Jaehun Han, Jun Beom Kim, Dong Yun Lee, Sung Min Cho, Jeong Ho Cho, J. Phys. Chem. C, 120 (2016), 22012 - 22018.

[45] Jonathan S. Alden, Haixia Dai, Michael R. Knapp, Shuo Na, Hash Pakbaz, Florian Pschenitzka, Xina Quan, Michael A. Spaid, Adrian Winoto, Jeffrey Wolk. Transparent Conductors Comprising Metal Nanowires, U.S. Patent 8,049,333 B2. Nov. 1, 2011.

[46] Kwonwoo Shin, Ji Sun Park, Jong Hun Han, Yunsu Choi, Dae Sung Chung, Se Hyun Kim, Sci. Rep, 7 (2017), 40087.

[47] Sidney T. Malak.; Guanquan Liang.; Ramathasan Thevamaran.; Young Jun Yoon.; Marcus J. Smith.; Jaehan Jung.; Chun Hao Lin.; Zhiqun Lin.; Edwin L. Thomas.; Vladimir V. Tsukruk. *J. Phys. Chem. C*, 2017, *121*, 13370–13380.

[48] Seung-Kyu Park.; Xuecheng Teng.; Juhyung Jung.; Prem Prabhakaran.; Cheol Woo Ha.; Kwang-Sup Lee. *Opt. Mater. Express*, 2017, 7, 2440-2449.

[49] Garcia-Vaquero, M. Rajauria, G. O'Doherty, J.V., Sweeney, T., Food Research International, 2017, 99, 1011-1020

[50] Suslick, K. S., Flannigan, D. J., Sonochemistry, Science, 1990, 247, 1439-1445.

[51] Suslick, K. S., Flannigan, D. J., Inside a Collapsing Bubble, Sonoluminescence and Conditions during Cavitation, Annu. Rev. Phys. Chem., 2008, 59, 659-683.

[52] Peshkovsky, A. S., Peshkovsky, S. L., Bystryak, S., Scalable high-power ultrasonic technology for the production of translucent nanoemulsions, Chemical Engineering and Processing, Process Intensification, 2013, 69, 62-77.

[53] Golmohamadi, Amir, Effect of ultrasound frequency on antioxidant activity, total phenolic anthocyanin content of red raspberry puree, Ultrasonics Sonochemistry, 2013, 20, 1316-1323.

[54] Wan Ki Bae.; Kookheon Char.; Hyuck Hur.; Seonghoon Lee. *Chem. Mater.* 2008, *20*, 531–539.

[55] Christian Würth.; Markus Grabolle.; Jutta Pauli.; Monika Spieles.; Ute Resch-Genger**.** *Nat. Protoc*, 2013, 8, 1535-1550.

[56] Yi Shen.; Rui Tan.; Megan Y. Gee.; Andrew B. Greytak. *ACS Nano*, 2015, 9,

3345-3359.

[57] Chon, J. W. M.; Zijlstra, P.; Gu, M.; Van Embden, J.; Mulvaney,P. *Appl. Phys. Lett*, 2004, 85, 5514−5516.

[58] Asami, H.; Abe, Y.; Ohtsu, T.; Kamiya, I.; Hara, M. *J. Phys. Chem. B*, 2003, 107, 12566−12568.

[59] Arjan J. Houtepen.; Zeger Hens.; Jonathan S. Owen.; Ivan Infante. *Chem. Mater*, 2017, 29, 752−761.

[60] Jon M. Azpiroz.; Filippo De Angelis. *ACS Appl. Mater. Interfaces*, 2015, 7, 19736−19745.

[61] Michael M. Krause.; Lakshay Jethi.; Timothy G. Mack.; Patanjali Kambhampati. *J. Phys. Chem. Lett*, 2015, 6, 4292−4296.

[62] Bao, H.; Gong, Y.; Li, Z.; Gao, M. *Chem. Mater*, 2004, 16 (15), 3853−3859.

Publication

[1] International Journals

1. Seonwoo Lee, Changhee Lee, High-Density Quantum Dots Compositions and Its Photolithographic Patterning Applications, *Polymer Composites*, submitted.

2. Seonwoo Lee, Kunsik An, Changhee Lee, Etchant-Free Photolithographic Patterning of Silver Nanowires Using UV Curable Resins and Ultra-Sonication, *Thin Solid Film,* In revision.

[2] International Conferences

1. Seonwoo Lee, Kunsik An, Changhee Lee, Etchant-Free Photolithographic Patterning of Silver Nanowires Using UV Curable Resins and Ultra-Sonication, International Conference on Science and Technology of Synthetic Metals (ICSM), Poster Session Ⅲ, Paper Number: 03_1028, July 5, 2018.

한글 초록

전도성 나노 물질 및 양자 구속 영역에 있는 반도체를 패터닝 하는데 있어서, 고전적인 포토 리소그래피 방법은 높은 생산성, 고해상도 및 대형화가 쉽다는 많은 이점을 제공 할 수 있다. 그러나, 나노 물질의 경우 포토 리소그래피 공정에 적용하는 데는 많은 어려움이 따른다. 즉, 패터닝 공정 동안 재료 안정화, 습식 코팅 솔루션에서의 분 산성, 화학적 및 기계적 불안정성으로 인한 물리적 박리 등이다. 본 연구에서는 우수한 광학 투명성과 낮은 굴절률을 갖는 수 불용성 고분자 (polymethylmethacrylate (PMMA))와 유기 용제의 감광성 가교제로 구성된 제형을 설계했습니다. 포토 마스크에서 UV 경화를 진행하고 유기 용매로 현상 한 후, 노출되지 않은 부분에서 AgNW 를 세척하기 위해 짧은 물 세척과 짧은 초음파 처리의 수행 및 효과를 비교하였다. 얻어진 AgNW 의 미세 패턴의 경우 가교 결합 된 폴리머 매트릭스로 보호되어 있으며, AgNW 의 폭은 100 ~ 3 ㎛ 범위 였고, 보호 된 AgNW 네트워크는 테이핑 및 굽힘 시험 후에도 우수한 기계적 안정성을 유지함을 확인 하였다. 응용 및 확장성을 살펴 보기 위하여, 본 연구는 미래의 플렉시블 전자 디바이스의 핵심 구성 요소 인 유기 트랜지스터에 개발 된 패터닝 방법을 적용하여 보았다. 0-D 구조 (예를 들어, 구, 클러스터)와 비교하여, 높은 종횡비를 갖는 1 차원 (1-D) 나노 와이어는 전극이 구부러 지거나 길어질 때 전도성 물질 사이의 연결을 위한 더 나은 기회를 제공하는 것으로 알려져 있다. 본 연구에서 연구되어진 물리적 패터닝 방법의 유용성을 확인하기 위해, 유기 전계 효과 트랜지스터를 제작하고 이를 Ag 금속으로 구성된 레퍼런스 디바이스와 비교했다.

다른 형태의 양자점으로서 최근 차세대 디스플레이 기술에 적용하고자 많은 연구가 되어 지고 있는 도트 형태의 나노 재료인 양자점 (예 : CdSe @ ZnS)와 같은 나노 물질에 대한 광 패턴화 방법도 병행해서 제안하고자 한다.

본 연구는 광 패턴 가능한 양자점 분산제형을 연구하였다. 이들 제형은 광 반응성 가교 결합제, 분산제 및 기타 첨가제를 갖는 상업용 중합체에 의해 혼합되어 패터닝 공정에 용이하게 적용되었다.

본 연구는 고 농도의 QD 분산과 고전적인 포토 리소 그래픽 패터닝 응용에 적용이 가능함을 보이고자 한다. 먼저 QD 분말과 상업용 분산제를 사용하여 저 농도로 QD 블렌딩을 고찰하였다. 그런 다음 추가 첨가제를 사용하여 고 농도의 QD 블렌딩 (최대 30 wt %)할 수 있는 방법을 연구하였다. 다음으로, 필름 공정 동안 발생 할 수 있는 양자점의 특성 변화, 예를 들면, PLQY 와 광학 특성, 등의 특성들이 안정적 유지되는 지를 평가하였다. 마지막으로, 색 변환 필름에 적용 할 수 있는 고농축 QD (20wt % 이상)로 구성된 미세 패턴 이미지를 제시하였다.